LEVEL

12

P.S.

AD A072144

INVESTIGATION OF MICROTUBULAR CERAMIC STRUCTURES

Robert L. Fullman
Corporate Research and Development
General Electric Company
P.O. Box 43
Schenectady, New York 12301

February 1979

Final Report for Period 1 July 1976 - 31 January 1979

Prepared for

OFFICE OF NAVAL RESEARCH
Material Sciences Division
Arlington, Virginia 22217

SRD-79-018

79 07 31 041

Unclassified

SECURITY CLASSIFICATION OF THIS PAGE (When Data Entered)

REPORT DOCUMENTATION PAGE	READ INSTRUCTIONS BEFORE COMPLETING FORM
1. REPORT NUMBER	2. GOVT ACCESSION NO. 3. RECIPIENT'S CATALOG NUMBER
4. TITLE (and Subtitle) (6) INVESTIGATION OF MICROTUBULAR CERAMIC STRUCTURES	(9) 5. TYPE OF REPORT & PERIOD COVERED Final Report, 1 July 1976 - 31 January 1979 6. PERFORMING ORG. REPORT NUMBER (14) SRD-79-018
7. AUTHOR(s) (10) Robert L. Fullman	(15) 8. CONTRACT OR GRANT NUMBER(s) N00014-76-C-1047
9. PERFORMING ORGANIZATION NAME AND ADDRESS Corporate Research and Development General Electric Company P.O. Box 43 Schenectady, New York 12305	10. PROGRAM ELEMENT, PROJECT, TASK AREA & WORK UNIT NUMBERS
11. CONTROLLING OFFICE NAME AND ADDRESS Office of Naval Research Material Sciences Division Arlington, Va. 22217	(11) 12. REPORT DATE February 1979 13. NUMBER OF PAGES 94
14. MONITORING AGENCY NAME & ADDRESS(if different from Controlling Office) (12) 96 p.	15. SECURITY CLASS. (of this report) Unclassified 15a. DECLASSIFICATION/DOWNGRADING SCHEDULE

16. DISTRIBUTION STATEMENT (of this Report)

Distribution Unlimited

17. DISTRIBUTION STATEMENT (of the abstract entered in Block 20, if different from Report)

18. SUPPLEMENTARY NOTES

Project Manager - Code 473/Mr. Kieth Ellingsworth

19. KEY WORDS (Continue on reverse side if necessary and identify by block number)

Ceramics	Microtubes
Foams	Microtubular ceramics
Heat Exchangers	Microtubular structures
Heat transfer	

20. ABSTRACT (Continue on reverse side if necessary and identify by block number)

Calculations and experiments were conducted to explore the feasibility of producing very compact high-temperature heat exchangers via microtubular ceramic structures. Such microtubular ceramic structures consist of multiple interconnected ceramic tubes with very thin walls, small diameters, and modest ratios of length to diameter. As a result, they should have reasonable strength, as well as very high specific area. The investigation included: calculations of expected volume requirements and heat-exchange performance

DD FORM 1 JAN 73 1473 EDITION OF 1 NOV 65 IS OBSOLETE

Unclassified 406 617

SECURITY CLASSIFICATION OF THIS PAGE (When Data Entered)

79 07 31 041

20. Abstract (Cont'd)

for microtubular ceramic heat exchangers compared to ones of conventional dimensions; experiments seeking to define means for preparing leak-tight microtubular ceramic structures; preliminary exploration of means to provide separate manifolds to the interior and exterior of the microtubes; and a leak test of one experimental manifold microtubular ceramice structure.

GENERAL ELECTRIC

ACKNOWLEDGMENTS

Many of the author's colleagues have provided valued advice during the course of this investigation, but repeated consultations by Drs. S. Prochazka, J.E. Burke, K.W. Lay, L. Navias, and R.W. Powers were particularly helpful. Dr. H.B. Vakil assisted greatly in initial phases of the heat transfer analyses.

TABLE OF CONTENTS

Section		Page
1	INTRODUCTION	1
2	BACKGROUND	5
	Preliminary Heat-transfer Analysis	5
	Substrate Preparation	5
	Ceramic Coating Process	7
3	HEAT-TRANSFER CALCULATIONS	9
	Materials Suitability	9
	Full Heat-exchanger Calculation	10
	Temperature Limits	12
	Sensitivity to Assumptions	13
4	CERAMIC COATING EXPERIMENTS	17
	Experimental Procedure	17
	Step 1. Adhesive Application	17
	Step 2. Formation of Packed-Powder Bed	17
	Control of Powder Pressure	18
	Step 3. Vibration Period	19
	Step 4. Loose Powder Removal	19
	Step 5. Consolidation	20
	Coating Evaluation	20
	Adhesive Thickness	20
	Fired-ceramic Thickness	21
	Coating Results: Aluminas and Zirconia	22
	Comments and Visual Observations	24
	Experiments 01x — Lucalox Analog (Powder A)	24
	Experiments 02x — Lucalox Analog (Powder A)	25
	Experiments 03x — Linde C (Powder B)	25
	Experiments 04x — Norton 38-900 (Powder C)	25
	Experiments 05x — Excel "3-5 CAL" (Powder D)	25
	Experiments 06x — Excel "3-5 CAL" (Powder D)	26
	Experiments 07x — Stabilized Zirconia (Powder E)	26
	Experiment 081 — Reynolds RC-HP (Powder F)	26
	Experiment 091 — Meller CR10 (Powder G)	27
	Experiment 101 — Calcined Meller CR10 (Powder H)	27
	Experiments 11x — Excel "3-5 CAL" (Powder D)	27
	Characterization of Alumina Powders	27
	Conclusions from Alumina Coating Experiments	28
	"Conventional" Ceramic Compositions	31
	Packed-Bed Powder Coating Results	38

TABLE OF CONTENTS (Cont'd)

Section		Page
	Comments and Visual Observations	38
	Experiments 12x — Calcined Kyanite (Powder I)	38
	Experiments 13x — Sierra Talc No. 1 (Powder J)	40
	Experiments 14x — Kentucky Ball Clay (Powder K)	40
	Experiments 15x — E. P. Kaolin (Powder L)	40
	Experiments 16x — 38-400 Alumina (Powder M)	40
	Experiments 17x — Volclay Bentonite (Powder N)	40
	Experiments 18x — F-202 Forsterite (Powder O)	41
	Experiments 19x — Treasure Talc (Powder P)	41
	Experiments 20x — Feldspar (Powder Q)	41
	Experiments 21x — C-70 Forsterite (Powder R)	41
	Experiments 22x — Silica (Powder S_1)	41
	Experiments 23x — Silica (Powder S_2)	42
	Experiments 24x — Silica (Powder S_3)	42
	Experiments 25x — Calcined Magnesite (Powder T)	43
	Experiments 26x — Pseudo-Kaolin (Powder U)	43
	Experiments 27x — 30-μm Minusil (Powder S_4)	43
	Experiments 28x — 10-μm Minusil (Powder S_5)	43
	Experiments 29x — "Electrical Insulator" (Powder V)	44
	Experiments 30x — "Parian" (Powder W)	44
	Experiments 31x — F-202 Forsterite (Powder O)	44
	Characterization of Selected Powders	44
	Reformulation of Ceramic Compositions	51
	Powder Coating Conclusions	55
5	FIRING EXPERIMENTS	57
	Procedures	57
	Results	58
6	MANIFOLDING EXPERIMENTS	67
	Preliminary Experiments on Ceramic Paste Suspensions	67
	Tube-exterior Manifolds: Preliminary Experiments	72
	Preparation of Samples for Leak Testing	73
	"Electrical Insulator"	73
	"Parian"	74
	F-202 Forsterite	76
7	FIRING OF LEAK TEST SAMPLES	79
8	LEAK TESTING	83

TABLE OF CONTENTS (Cont'd)

Section		Page
9	SUMMARY AND CONCLUSIONS	87
	Summary	87
	Conclusions	89
10	REFERENCES	91
11	DISTRIBUTION LIST	93

LIST OF ILLUSTRATIONS

Figure		Page
1	Schematic illustration of process for preparing microtubular ceramic structure with separate manifolds for access to exterior and interior of microtubes.	2
2	Schematic diagram of a microtubular ceramic structure applied as a heat exchanger element.	3
3	Schematic diagram of an array of four microtubular heat-exchanger elements and connecting passages.	3
4	Process steps for rounding fibrils of open-cell foam.	6
5	Compression test results on polyurethane foam pad used to provide pressure in early packed-bed powder coating experiments.	19
6	Electron micrograph of Excel "3-5 CAL" alumina (powder D).	29
7	Electron micrograph of Lucalox mix (powder A).	29
8	Electron micrograph of Excel 1-μm alumina polishing powder.	30
9	Electron micrograph of Excel 0.3-μm alumina polishing powder.	30
10	Electron micrograph of E.P. Kaolin (powder L).	45
11	Electron micrograph of Kentucky ball clay (powder K).	46
12	Electron micrograph of Volclay bentonite (powder N).	46

LIST OF ILLUSTRATIONS (Cont'd)

Figure		Page
13	Electron micrograph of Sierra talc No. 1 (powder J). . . .	47
14	Electron micrograph of K-200 feldspar (powder Q).	47
15	Electron micrograph of 10-μm Minusil (powder S_5).	48
16	Electron micrograph of "electrical insulator" powder mixture (powder V).	48
17	Electron micrograph of "Parian" powder mixture (powder W).	49
18	Electron micrograph of calcined kyanite (powder I).	49
19	Electron micrograph of 38-400 alumina (powder M).	50
20	Electron micrograph of F-202 forsterite (powder O). . . .	50
21	Chips from calcined kyanite microtubular ceramic sintered one hour at 1600 ^{o}C.	59
22	Sintered calcined kyanite: a) tap-dense, then fired at 1600 ^{o}C; and b) loose powder, fired at 1700 ^{o}C.	60
23	Sintered calcined kyanite first pressed at 69 MPa then sintered at a) 1600 ^{o}C and b) 1700 ^{o}C.	61
24	Tap-dense F-202 forsterite fired at 1550 ^{o}C.	63
25	Tap-dense "electrical insulator" fired at 1385 ^{o}C.	63
26	Tap-dense "Parian" fired at 1300 ^{o}C.	64
27	Room-temperature evaporation of liquid from single-side coatings of paste suspensions on powder-coated foam samples.	71
28	Drying cracks on top face of F-202 forsterite paste suspension coating.	77
29	"Open" faces of "electrical insulator" microtubular structure after firing at 1419 ^{o}C.	80
30	Bored-out face of "electrical insulator" microtubular sample.	84

LIST OF TABLES

Table		Page
1	Calculated Thermal Characteristics of Heat-Exchangers. . .	11
2	Calculated Thermal Limits of Heat Exchangers	13
3	Sensitivity of Calculated Heat-Exchanger Characteristics to Assumed Parameters and Calculation Method	14
4	Quantitative Results of Alumina Powder-Coating Experiments	24
5	Quantitative Results of Al_2O_3-MgO-SiO_2 System Powder Coating Experiments	39
6	Particle Size Measurements on Selected Powders	51
7	Summary of Quantitative Information on Al_2O_3-MgO-SiO_2 System Powder Coating	51
8	Idealized Compositions of Selected Powders	53
9	Constituents Used in Formulating Some Typical Al_2O_3-MgO-SiO_2 System Ceramics	54
10	Calculated Alternate Formulations of Al_2O_3-MgO-SiO_2 System Ceramics, Employing Favorable Materials for Packed-Bed Powder Coating	55
11	Influence of Firing Temperatures on Ceramic Densities . . .	62

Section 1

INTRODUCTION

This study has been directed toward an exploration of the feasibility of fabricating very thin-walled, high-specific-area structures of multiply interconnected ceramic tubes, suitable for use as very compact static heat exchangers or other process equipment. The basic concept is to use a modified polymer foam as a sacrificial substrate which serves as a mold for the desired ceramic configuration. Ceramic processing steps are also envisaged to provide separate-access manifolds to the inner and outer surfaces of the tubes, so that the ceramic can separate a flow stream within the tubes from another that is outside of them.

The specific focus of the investigation has been on the preparation of tubes approximately 0.25 mm (0.010 inch) in diameter and 0.025 mm (0.001 inch) in wall thickness. Despite their thin walls, such ceramic tubes should have reasonable structural strength as a result of their small diameter and modest length/diameter ratios. The sacrificial substrate used to mold the tube interiors was an open-celled polyurethane foam, modified by an additional polymer coating to convert its originally triangular-section fibrils to circular cross sections. After deposition of a thin ceramic coating on the foam's fibrils, the polymer could be burned out during firing of the ceramic, leaving the desired interconnected array of small-diameter, thin-walled ceramic tubes.

The approach for providing selective access from a region of the microtubular structure's surface to the tube interiors was to apply a thick paste of a ceramic slip so as to form a continuous skin over that region. The excess ceramic paste would then be wiped off the surface so that the polymer substrate was either exposed or very near the surface; a light grinding after firing then opens this surface region to the interior passages of the tube array. Surfaces which were not given this special treatment during the ceramic application process would provide selective access to the flow region on the outside of the tubes.

Figure 1 illustrates schematically the process for forming the microtubular array by coating, sintering, and grinding. Figure 2 is a schematic diagram of an array element configured for use as a heat exchanger, using the hot gases from a combustion process passing through the tube-exterior flow region, and a helium manifold interface to the tube interiors of the subassembly. Figure 3 depicts an additional schematic diagram illustrating the stacking of four modules, where A_h is the hot gas entry and A_c is the cooled gas exit; and B_c and B_h are the cold and hot tube-interior manifolds for the helium gas.

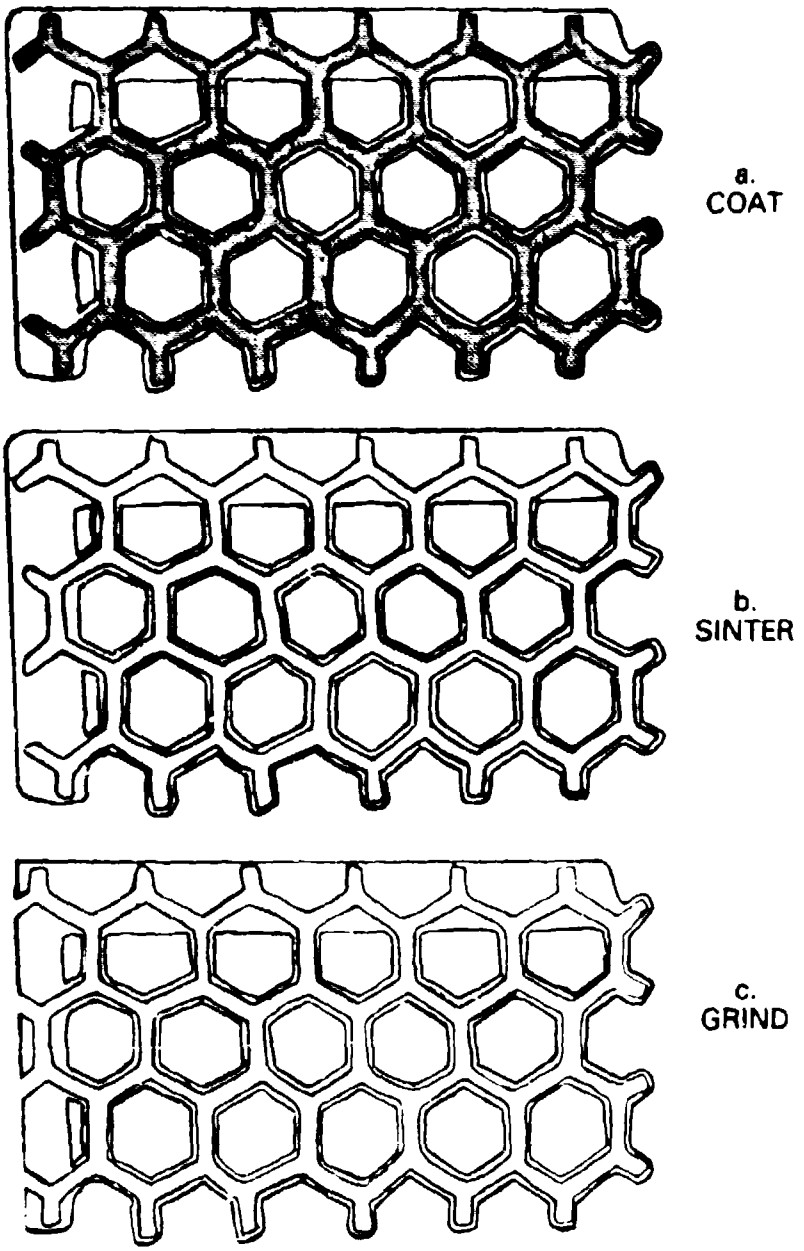

Figure 1. Schematic illustration of process for preparing microtubular ceramic structure with separate manifolds for access to exterior and interior of microtubes. a) Unfired ceramic coating over foam sacrificial substrate, with continuous ceramic paste coating two faces; b) sintered ceramic, with substrate burned out; and c) left face ground away sufficiently to expose access to tube interiors. Top face remains sealed: other faces provide selective access to tube exteriors.

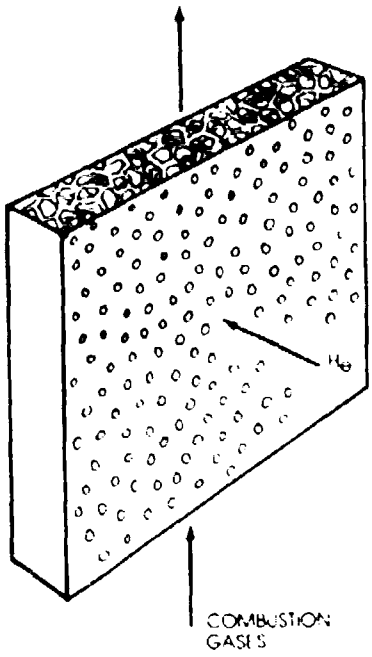

Figure 2.

Schematic diagram of a microtubular ceramic structure applied as a heat exchanger element. Large vertical faces have been processed (as in Figure 1, left face) to provide selective access to tube interiors; small vertical faces are sealed to define a cross-flow vertical passage on the tube exteriors; and horizontal faces are open to provide selective access to this tube-exterior flow path. Labels illustrate a possible heat exchange between combustion gases passing on the tube exteriors and helium passing through the tube interiors.

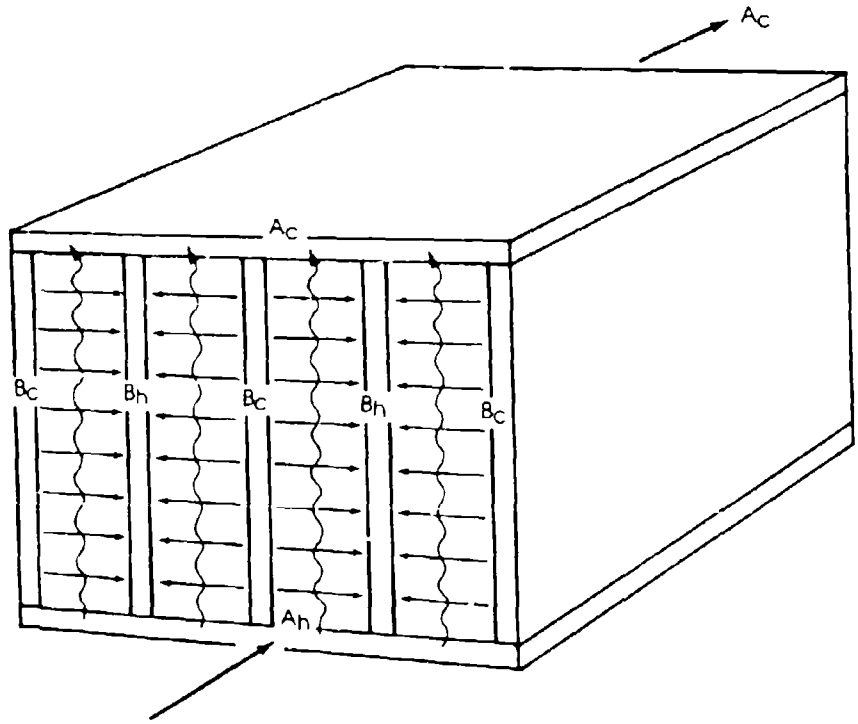

Figure 3. Schematic diagram of an array of four microtubular heat-exchanger elements and connecting passages.

Section 2

BACKGROUND

PRELIMINARY HEAT-TRANSFER ANALYSIS

Prior to this investigation, a preliminary and partial heat-transfer analysis [Ref. 1] was performed to test the hypothesis that a heat exchanger utilizing a microtubular structure could be designed so as to match the heat-transfer effectiveness of a conventional heat exchanger, with the same pressure drop and a smaller volume than the conventional unit. For simplicity, the analysis addressed only the tube-interior half of the heat exchanger, since this side is expected to be the limiting factor with respect to pressure drop. Calculations were made for a heat exchanger operating with helium at 40 atmospheres, ~ 1000 K, a 4.5-psi pressure drop, and 12.7-mm-(0.5-inch) diameter tubes 304.8 cm (10 feet) long, giving an estimated heat-transfer effectiveness of 97 percent.

The analysis indicated that a microtubular heat exchanger with 0.254-mm-(0.01-in.) inside diameter tubes would operate with the same pressure drop and heat-transfer effectiveness if it had an effective tube length of 25.4-mm (1 in.) and about 40 percent greater total cross-sectional area of tubes than the conventional heat exchanger. Stated qualitatively, the greater specific area of the microtubular heat exchanger permits the flow-path length to be so shortened that the pressure drop through its tiny — but short — tubes is the same as in conventional-sized tubes that are much longer. The potential advantage of the microtubular heat exchanger is greatly reduced total volume and weight. For typical tube packing in the conventional heat exchanger (estimated at an internal tube volume equal to 1/3 the total volume), the calculated volume required for the microtubular structure was 1/20 that of the conventional unit.

SUBSTRATE PREPARATION

Prior to commencing this investigation, a successful process had been developed for preparing the sacrificial substrate by rounding the triangular fibrils of polyurethane open-celled foam. The process consists of the following steps:

1. Apply a thin coating of adhesive, from solution or suspension.
2. Shake the adhesive-coated foam in a container with beads or powder of the polymer to be applied, then shake out the nonadhering excess.
3. Heat for a short time to smooth the coating.

Ref. 1 H.B. Vakil, An Analysis of the Foam Heat Exchanger, unpublished work.

Since the beads or powder form essentially a monolayer coating over the fibrils, the amount added per coating is governed primarily by the particle size of the beads or powder used. Particle size ranges have been defined that provide sufficient coating material to round the fibrils in a one-coat operation, as illustrated in Figures 4a, 4b and 4c. Specifics of the substrate preparation are presented below.

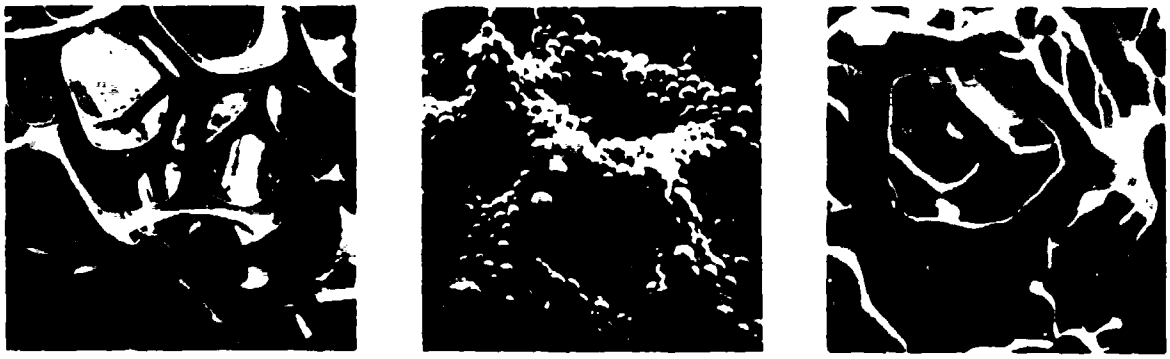

Figure 4. Process steps for rounding fibrils of open-cell foam. a. Uncoated polyurethane foam, b. foam coated with adhesive and adhering polymethyl methacrylate (PMMA) beads, and c. coated foam after heating 20 minutes at 245 ^{o}C.

Foam: ten pores-per-inch, polyurethane open-celled foam.

Adhesive: most commonly, Piccolyte S-10, a thermoplastic terpene resin composed mainly of polymers of beta-pinene was used. It was deposited by dipping the foam in a solution (e.g., 1 g S-10: 4 ml toluene), draining, and drying. Other adhesives have also been used.

Polymer Addition: Most commonly, polymethyl methacrylate (PMMA) (in the form of beads), a commercial product produced by emulsion polymerization, was used. Crushed powder of alpha-methyl styrene was also employed successfully. These polymers were chosen for their low decomposition temperatures, assuring that during subsequent heating (to sinter the ceramic coating) the outer polymer coating decomposes along with or before the polyurethane, thereby permitting free escape of the gaseous decomposition products. The polymer was most commonly applied by handshaking the adhesive-coated foam in a small jar partially filled with the polymer beads or powder, then shaking in an empty jar to remove any nonadhering particles. Particle sizes exceeding nominal 100 to 150 μm (U.S. Standard sieves, -100 +140 fraction) add sufficient polymer to fully round the fibrils of 10 pores-per-inch polyurethane foam. At a nominal particle size of 177 to 250 μm (-60 + 80 sieve fraction) or larger, too much polymer is added, leading to occasional closing of cell face openings during the subsequent smoothing operation. Satisfactory rounding of the fibrils could be obtained over an

approximately 2:1 range of the resulting fibril cross-sectional area, by changes in the polymer particle size, without changing the original foam.

Smoothing the Polymer: The adhering beads or powder were caused to flow into a smooth coating by heating, for 10 to 40 minutes at 220 to 245 ^{o}C for PMMA or at 110 to 130 ^{o}C for alpha-methyl styrene. Coarser beads or powder particles required a longer time and/or a higher temperature to flow sufficiently to form a smooth coating.

CERAMIC COATING PROCESS

Prior to commencing this investigation, a number of potential means were explored for preparing a controlled, uniformly thick coating of ceramic over the PMMA-coated foam* fibrils. Conventional coating methods using a liquid suspension of ceramic powder (slip) are unsuitable, since surface tension forces prevent forming a controlled, uniformly thick coating.

Of the potential coating methods explored, the most nearly successful one was a packed-bed powder coating process, described below. In general, it is a means for accreting dry powder to the foam fibrils, using a liquid adhesive. With this process, the desired general configuration had been produced and fired to a microtubular ceramic structure. However, the tube walls were quite porous; the ceramic material (stabilized zirconia) then under study required an extremely fine particle size (~ 0.4 μm) for satisfactory sintering. With zirconia powder of this particle size, spherical aggregates formed during the manipulations required in the packed-bed powder coating process and prevented formation of continuous coatings. During the investigation reported here, experiments were performed to determine whether a powder of some other ceramic, suitable for heat-exchanger applications, might be both sinterable and amenable to coating via the packed-bed powder coating process.

As a result of the experience gained during this investigation, some details of the packed-bed powder coating process were modified, but the general procedure always consisted of the following steps:

1. Dip the substrate after the above fibril rounding into a solution containing a viscous liquid adhesive and a volatile solvent, remove, drain, and dry.
2. Pack the adhesive-coated substrate in the powder to be coated onto it, in a closed container.
3. Vibrate the container for a period of time.
4. Remove the powder and the substrate, and shake any unattached powder from the foam substrate's interstices.

*PMMA-coated foam was used for all of the substrates employed in this investigation.

5. Heat the powder-covered sample at a temperature where the adhesive becomes fluid, but little evaporation or decomposition occurs.

6. Repeat steps 2 through 5, as required, until the desired thickness of the powder coating has been applied.

The following working hypotheses were used for initial definition of the process steps. It was assumed that:

- A more-than-sufficient supply of adhesive can be provided over the entire substrate surface, so that uniformity of the ceramic coating is not dependent upon precise uniformity of the adhesive.
- The principal mechanism of powder accretion is by diffusion of the adhesive from the substrate surface into the adjacent powder. Thus, primary control of the coating thickness would be the diffusion time (step 3).
- Surface tension of the impregnated adhesive may cause an increase in the packing density of the powder into which it has diffused. The container was vibrated in step 3 to promote the delivery of additional powder to the diffusion front in order to avoid formation of a gap.
- Heating the powder-covered sample (step 5) would cause the adhesive concentration to become substantially uniform throughout the coating thickness, thereby enhancing its mechanical integrity and the rate of additional adhesive diffusion in a repeat cycle.

Handling of the coated substrate during the procedures described above caused defects in the coating of the fibril tips at the substrate's macroscopic surface. It was recognized that additional process steps would be required to repair these surface defects, unless they could be prevented by more refined procedures. (Prevention or repair of uncoated tips on the substrate's outer surface were not a part of the initial exploration.) In general, the packed-bed powder coating process had been shown to be "operable", but it had not been established that the working hypotheses describe the actual mechanism of its operation. The prior studies had shown that success is sensitive to the powder's freedom from aggregates (or from too-large ones) and to its tendency to form aggregates during manipulation.

Section 3

HEAT-TRANSFER CALCULATIONS

MATERIALS SUITABILITY

The first task undertaken in this investigation was a theoretical examination of the suitability of various ceramic materials for use in high-performance microtubular heat exchangers, as a basis for selecting materials for the experimental program.

For a given set of materials properties, tube proportions (e.g., outer-to-inner radius ratio b/a), and specific thermal flux $\dot{q}$ (=$\dot{Q}$/A), the steady-state thermal stress is proportional to the tube wall-thickness δ. Hence, the small dimensions of a microtubular structure may permit the use of materials that would be overstressed in a heat exchanger constructed of larger tubes. The maximum* tensile stress occurs at the cooled wall surface, and is given by [Ref. 2].

$$\sigma_\theta = \sigma_z = \frac{E\alpha\dot{q}\delta\ f(b/a)}{(1-\nu)\ K} \qquad (1)$$

where E, ν, α, and K are the materials' Young's modulus, Poisson's ratio, thermal-expansion coefficient, and thermal conductivity; and f(b/a) ≈ 0.48 for b/a = 1.2 (a typical value for structurally strong ceramic tubes). Hence, a comparison of the quantity $E\alpha\delta/(1-\nu)K$ for various materials, with δ appropriate to either conventional or microtubular structures, provides a first indication of the relative importance of the geometry and the material properties with respect to thermal stress limitations. A comparison was made for the following materials: 1) silicon carbide (SiC) and 2) silicon nitride (Si_3N_4), both materials of current interest for demanding thermal applications, but still in a developmental status, 3) beryllium oxide (BeO), an established high-conductivity ceramic, but requiring special process considerations due to health hazards, 4) zircon ($ZrSiO_4$), a refractory with excellent thermal shock resistance, but having limited usage in a high-density form since its maximum sintering temperature is limited by thermal decomposition, 5) alumina (Al_2O_3), quite refractory, not having exceptional thermal shock resistance, but well documented with respect to processing technology and properties; and 6) stabilized zirconia (Y_2O_3/ZrO_2), quite refractory, but difficult to sinter. The latter material is included since the prior microtubular structures work was done with this ceramic.

*Higher stresses may occur at tube ends and junctions and during thermal transients, but are less readily calculated and sensitive to design details. Equation 1 should serve for comparing materials.

Ref. 2. S. P. Timoshenko and J. N. Goodier, Theory of Elasticity, 3d edition, McGraw-Hill Book Company, New York, 1970.

Taking 1.27 mm (0.05 inch) as the wall-thickness for the "conventional" tubes and 0.0254 mm (0.001 inch) for the microtubular tubes, the values of $E\alpha\delta/(1-\nu)K$ for the six materials are:

Tubes	SiC	Si_3N_4	BeO	$ZrSiO_4$	Al_2O_3	ZrO_2
Conventional, N/W	70	130	150	220	640	1500
Microtubular	1.4	2.6	2.9	4.3	12.8	29.9

Thus, if all else were equal, the steady-state thermal stress level for the poorest of these materials (ZrO_2) in a microtubular structure would be less than that for the best material (SiC) in conventional-size tubes.

FULL HEAT-EXCHANGER CALCULATION

In order to assess whether typical inequalities in the "all else" state referred to above might negate much of the advantage of thin tube walls, a full calculation was made of the thermal and stress characteristics of a hypothetical "conventional" heat exchanger and a microtubular unit, using the six materials listed above and established fluid dynamics and heat-transfer relationships [Refs. 3, 4]. This calculation also provides insight into the likelihood that thermal stress would actually be a limiting consideration, and the significance of the materials' thermal conductivities to thermal performance of the heat exchangers. No particular application was considered in selecting the heat exchange fluids, temperatures, pressures, etc., and the results will not apply exactly to heat exchangers designed for other values of these parameters or with other specific configurations. They should indicate approximately the expected general characteristics of other gas/gas heat exchangers, particularly with respect to the relative suitability of various materials.

The calculation built upon a partial calculation [Ref. 1] (tube interior only) performed earlier and submitted as part of the proposal that led to this contract. As in that calculation, the interior fluid was taken to be helium at 40 atmospheres pressure and a mean temperature of 1000 K; the "conventional" tubes had an inside diameter of 12.7 mm (0.5 inch) and were 304.8 cm (10 feet) long, they occupied 1/3 of the total volume, and the mass flow rate through them was 15 $g/cm^2 \cdot s$; the microtubular structure was assumed to have 0.254-mm (0.01 inch) inside diameter tubes, occupying 1/13 of the total volume, and to have the mass flow rate (10.8 $g/cm^2 \cdot s$) and the L/D

Ref. 3 J. G. Knudsen and D. L. Katz, Fluid Dynamics and Heat Transfer, McGraw-Hill Book Company, New York, 1958.

Ref. 4 W. H. McAdams, Heat Transmission, 3d edition, McGraw-Hill Book Company, New York, 1954.

ratio (95) required to match the (interior) heat-transfer effectiveness factor and the pressure drop of the "conventional" size tubes. Additional assumptions made for the full calculation were: an exterior fluid, air at one atmosphere, and a mean temperature of 800 K; the tube wall-thickness equaled 1/10 of the inside diameter; the external pressure drop was the same as the interior drop (30.6 kPa, or 4.44 psi). The "conventional" heat exchanger was designed as a single-pass, baffled, counterflow exchanger with matched exterior and interior thermal loads (mass flow times heat capacity). In recognition of likely limits in configuring the flow paths of microtubular structures, this exchanger was designed as a cross-flow unit having an external path length equal to the interior path (2.41 cm), with the thermal load unbalanced as required to meet the stipulated pressure drop.

For each tube material, the calculated thermal characteristics of the "conventional" and microtubular heat exchangers are listed in Table 1. The characteristics given are the overall mean heat-transfer coefficient $\overline{U}_i$ (referred to tube-interior area), the effectiveness factors* η_H for heating and η_c for cooling, and the specific volume* V_o.

Table 1

CALCULATED THERMAL CHARACTERISTICS OF HEAT-EXCHANGERS

	SiC	Si_3N_4	BeO	$ZrSiO_4$	Al_2O_3	ZrO_2
Conventional						
$\overline{U}_i$, $\frac{W}{cm^2 \cdot {}^oC}$	0.0374	0.0365	0.0373	0.0337	0.0357	0.0312
$\eta_H (= \eta_c)$	0.315	0.310	0.315	0.294	0.306	0.278
V_o, $\frac{cm^3}{W/{}^oC}$	37.2	37.8	37.2	40.0	38.4	42.2
Microtubular						
$\overline{U}_i$, $\frac{W}{cm^2 \cdot {}^oC}$	0.137	0.137	0.137	0.136	0.137	0.135
η_H	0.573	0.572	0.573	0.570	0.572	0.568
η_c	0.374	0.372	0.373	0.371	0.373	0.369
V_o, $\frac{cm^3}{W/{}^oC}$	1.50	1.50	1.50	1.51	1.51	1.51

*For $\dot{q}$ (W/cm^2) specific thermal flux, t_1' and t_2' the initial and final air temperatures, and t_1'' and t_2'' the initial and final helium temperatures, $\eta_H \equiv (t_2'-t_1')/(t_1''-t_1')$; $\eta_c \equiv (t_1''-t_2'')/(t_1''-t_1')$; $V_o \equiv V(t_1''-t_1')/\dot{q}$. Thus, the effectiveness factors for heating and cooling are the fraction, of the maximum possible, that the respective gases are heated or cooled; and the specific volume is normalized to the heat-transfer per unit initial temperature difference.

Conclusions concerning the thermal characteristics are:

- For the materials considered, the choice of material had only minor influence on the thermal performance of a "conventional" gas/gas exchanger, and had negligible influence on that of a microtubular unit.
- Despite the unbalanced thermal loading required to meet the prescribed pressure drop with a reasonable path length, both the heating and cooling effectiveness factors for the microtubular heat exchanger exceeded that of the "conventional" unit.
- The specific volume of the microtubular heat exchanger was smaller than that of the "conventional" unit by a factor of ~ 25 to 29, depending on the material used.

TEMPERATURE LIMITS

Omitting considerations such as permeation or corrosion (which are specific to particular applications and choice of fluids), the maximum initial temperature difference of the heat exchange fluids might be taken as a measure of the severity of conditions under which the exchanger's material can survive. This temperature difference Δ_{max} ($= t_1''-t_1'$) may be limited either by the thermal stress produced by the resulting heat flux or by a maximum temperature limitation of the material, e.g., due to melting, decomposition, or evaporation. For each of the materials examined here, a maximum temperature limit T_L was taken as 0.7 times the absolute temperature of melting or 0.9 times the temperature of appreciable decomposition or evaporation, whichever is lowest. Then, assuming that the initial coolant temperature t_1' in a high-temperature heat exchanger is unlikely to be lower than room temperature, the relative values of the solid and two gas-phase components of the overall heat-transfer coefficient determine a maximum initial temperature difference Δ_T permitted by the solid's temperature limit T_L. The possibility that the material's usefulness is limited by thermal stress may then be evaluated by calculating the value σ_{max} corresponding to this maximum fluids-temperature difference*. If the calculated stress exceeds a limiting value (taken here as 150 MPa (~ 22 ksi) to allow a reasonable margin for end-effects, etc.), a reduced temperature difference Δ_σ, permitted by the thermal stress criterion, is the appropriate measure of survivable severity. Results of the calculation are given in Table 2. The results of this calculation are summarized below. For the parameters assumed:

- Steady-state thermal stress limits the maximum fluids temperature-difference only for alumina or stabilized zirconia in "conventional"

*σ_{max} is calculated using the maximum heat-transfer coefficient corresponding to the forward stagnation point in the coolant flow.

Table 2

CALCULATED THERMAL LIMITS OF HEAT EXCHANGERS

	SiC	Si_3N_4	BeO	$ZrSiO_4$	Al_2O_3	ZrO_2
T_L, °C	1755	1458	1717	1357	1353	1724
Conventional						
Δ_T, °C	1910	1580	1870	1460	1460	1850
σ_{max}, MPa	26	38	52	54	170	430
Δ_σ, °C	--	--	--	--	1300	650
Microtubular						
Δ_T, °C	1960	1620	1910	1510	1500	1920
σ_{max}, MPa	3	4	6	7	20	58
Δ_σ	--	--	--	--	--	--

size tubes and for none of the materials in microtubular heat exchangers.

- The maximum permissible fluids temperature-difference is slightly greater for a microtubular heat exchanger than for a "conventional" heat exchanger made with the same material.

SENSITIVITY TO ASSUMPTIONS

All of the calculations described above assumed as interior fluid, He at 40 atmospheres pressure and a mean temperature of 1000 K and, as exterior fluid, air at one atmosphere and a mean temperature of 800 K. In view of the uncertainty in extending the semiempirical multitube heat-transfer relations to vastly different proportions and scale from their experimental basis, the calculations were made using equations describing single-tube heat transfer, but with the gas velocity taken as the maximum in the assumed configurations. The thermal limit Δ_T was calculated using the average value of the external heat-transfer coefficient, while the steady-state stress σ_{max} was calculated using the maximum coefficient corresponding to the forward stagnation point in the coolant flow. Longitudinal and tangential heat fluxes in the material were not considered.

In order to test the sensitivity of the conclusions to these assumptions, calculations were performed for several variants of the assumed parameters or computation method, using Al_2O_3 as the assumed material. The results are summarized in Table 3.

Table 3

SENSITIVITY OF CALCULATED HEAT-EXCHANGER CHARACTERISTICS TO ASSUMED PARAMETERS AND CALCULATION METHOD

	$\bar{U}_i$	η_H	η_c	V_o	Δ_T	σ_{max}	Δ_σ
	$W/(cm^2 \cdot {}^oC$			$cm^3/(W/{}^oC)$	(^oC)	(MPa)	(^oC)
External Fluid, air at 1 atmosphere, 800 K (1st calculation)							
Conventional	0.0357	0.306	0.306	38.4	1460	170	1300
Microtubular	0.137	0.572	0.372	1.51	1500	20	--
External Fluid, air at 40 atmosphere, 800 K							
Conventional	0.0738	0.476	0.476	24.6	1550	210	1110
Microtubular	0.215	0.521	0.521	1.07	1660	31	--
External Fluid, Helium at 40 atmosphere, 800 K							
Conventional	0.107	0.569	0.569	20.1	1590	280	860
Microtubular	0.347	0.617	0.617	0.91	1790	45	--
Multitube Heat-transfer Equations (original coolant)							
Conventional	0.0494	(0.368 to 0.378)		31.0-31.9	1500	200	~ 1110
Microtubular	0.145	0.586	0.381	1.47	1510	24	--
Multitube Equations, Δ_T based on minimum local heat-transfer coefficient							
Conventional	--	--	--	--	1380	185	~ 1110
Microtubular	--	--	--	--	1410	23	--

Improving the assumed heat-transfer properties of the coolant by pressurizing to 40 atmospheres improves the predicted thermal performance of both heat exchangers, the conventional configuration slightly more than the microtubular unit. The ratio of their specific volumes drops from about 25 to 23. (The slight reduction in η_H for the microtubular exchanger with a pressurized coolant is due to assumed operation with a balanced thermal load, in order to increase η_c to an equal value. This option was precluded

with unpressurized air due to excessive pressure drop.) However, the improved coolant characteristics reduce the maximum initial temperature difference Δ_σ for the conventional geometry by 190 ^{o}C; the microtubular exchanger remains thermally limited, rather than stress limited, so the improved coolant increases its limit Δ_T by 160 ^{o}C. Thus, in this respect, the predicted advantage of a microtubular configuration is increased from 200 ^{o}C with 1-atmosphere air to 550 ^{o}C with 40-atmosphere air as the coolant.

Further improvement of the coolant, by assuming the use of pressurized helium rather than air, leads to additional enhancement of the thermal performance predicted for both configurations. The predicted ratio of specific volumes becomes about 22. The microtubular advantage with respect to the maximum initial temperature difference is further increased to 930 ^{o}C.

The use of multitube heat-transfer relations [Ref. 4, 5] also leads to a slightly improved predicted thermal performance of both conventional and microtubular heat exchangers. The range of values of $\eta_H (=\eta_C)$ and V_o for the conventional configuration reflects uncertainty in the degree to which true counter-flow conditions may be approximated; the lower effectiveness factor and the larger specific volume correspond to assuming unmixed cross-flow.

Use of calculated minimum local heat-transfer coefficients [Ref. 6], rather than average values, leads to a similar reduction of the predicted Δ_T for both "conventional" and microtubular configurations. Since for Al_2O_3 the conventional-geometry exchanger is Δ_σ limited, this reduces the predicted advantage for the microtubular exchanger from 400 to 300 ^{o}C. In both instances, only radial heat flux was considered; hence, the Δ_T value predicted using the minimum local heat-transfer coefficient represents an appropriate approximation for very low-conductivity solids, while the Δ_T values calculated using the average coefficient should be a good approximation for high-conductivity solids, e.g., metals. A rough estimate of the tangential flux for Al_2O_3 indicates it may be comparable to the radial flux, so the proper value is intermediate between the two estimates. A more accurate evaluation would require numerical integration of the two-dimensional heat-flow equation.

Ref. 5 R. A. Bowman, A. C. Mueller, and W. M. Nagle, "Mean Temperature Difference in Design", Transactions of the ASME, Vol. 62, 1940, p. 283.

Ref. 6 A. S. T. Thomas et al., "Variation in Heat-transfer Rates Around Tubes in Cross Flow", Proceedings of the General Discussion on Heat Transfer, The Institution of Mechanical Engineers, 1951, p. 177.

In view of all of the calculations, it was concluded that:

- High-performance microtubular heat exchangers, exceeding the capabilities of "conventional" units, might be prepared using any of the materials considered.
- Process investigations using stabilized zirconia (initiated for solid-electrolyte fuel cell goals) would, if successful, also be useful for heat-exchanger goals.
- The most attractive material of those examined, considering processing background knowledge as well as predicted performance, is Al_2O_3.
- In view of the predicted performance benefits from microtubular configuration, lower-performance materials with process technology advantages also warrant consideration. (Calculations were not made for such materials (e.g., high-grade porcelains), since insufficient information could be found on their thermal and mechanical properties.)
- The qualitative conclusions are not altered by a considerable variation of the assumed operating parameters or by the use of alternative computation methods.

Section 4

CERAMIC COATING EXPERIMENTS

All of the ceramic coating experiments were conducted using the packed-bed powder-coating process and the PMMA-coated foam substrates, as generally described earlier. In order to conserve time in preparing PMMA-coated foam samples, a procedure was developed for removing the zirconia coatings from samples used in previous studies. It was found that substantially all of the previous coating was removed by a sequence of ultrasonic cleaning, 20 minutes in heptane, 30 minutes in detergent/water, and repeat. A "Bransonic 12" ultrasonic cleaner was used, with the samples and cleaning fluid contained in a 100-ml beaker dipping into the water-filled cleaner basin.

EXPERIMENTAL PROCEDURE

STEP 1. ADHESIVE APPLICATION

The adhesive used in all of the experiments was Hercules Corporation's Piccolyte S-10, a thermoplastic terpene resin composed mainly of polymers of beta-pinene. Previous experiments had indicated that adhesive coatings up to an estimated average thickness* of about 17 μm could be applied without encountering difficulties with adhesive blobs or bridges across the foam cell openings. There was a tentative association of relatively thick adhesive coatings with a type of defect in which regions of the substrate were completely bare of ceramic and remained bare on repeated coating cycles. This suggested that patches of the ceramic plus the adhesive might have come off the substrate. Coatings had been prepared using adhesive layers down to about 7 μm. (For context, if the ceramic powder deposit were composed of closely packed uniform spheres and if accretion required full occupancy of the interstices, a 9-μm layer of adhesive would be required to accrete enough powder for a desired 25-μm ceramic coating.) In the current experiments, the adhesive was deposited by dipping the sample for about 10 seconds in a solution of 4-ml heptane/g S-10; draining for one minute with occasional inversion of the sample; exposing to a compressed air blast, gradually bringing the sample to within 10 cm of the air-jet nozzle to break any cell-bridging adhesive films; and air drying for 30 minutes before weighing. The resulting coatings had estimated average thicknesses ranging from 9 to 13 μm.

STEP 2. FORMATION OF PACKED-POWDER BED

The adhesive-coated foam substrate was packed into the ceramic powder as follows: Powder was added to a 30-ml (1-oz) glass jar which was tapped

*Thickness estimates were based on weight gains, as described later.

on the tabletop to settle it, forming a powder bed approximately one fourth of the jar depth. The adhesive-coated foam substrate was placed on the powder bed, powder was added around the sides of the substrate, and the jar was tapped on the tabletop a few times to fix the substrate's position. More powder was then added, on top and around the substrate, with frequent tapping-in so that the powder level rose rather evenly through and around the substrate. When the substrate was completely impregnated and covered by powder, additional powder was added and tapped-in until the bed level was approximately at the point of the jar-neck constriction.

Control of Powder Pressure

In the early experiments, light powder pressure and resiliency of the pressure maintenance was varied qualitatively by placing one or more 0.32-cm (0.125-inch)-thick rubber disks atop the powder bed, varying the compression applied to a 1.27-cm (0.5-inch)-thick polyurethane foam disk placed under the jar lid. The results of these experiments suggested that the packing pressure is an important process variable, deserving more quantitative control.

In order to estimate the range of pressure levels used in these experiments, load-compression tests were made on the foam disk placed in a sandwich between two rubber disks, using an Instron testing machine, cross-head rate of 0.127 cm (0.05 inch)/min for a strain rate of ~ 0.10/min in the foam. Reproducibility was poor, and the unloading portion of the tests showed very large hysteresis. An additional test was made with periodic interruptions of the crosshead motion in order to observe the load relaxation. Figure 5 shows the pressure-strain results. Other experiments indicated a pressure of approximately 40 kPa (5.8 psi) at a foam thickness of 1 mm ($\epsilon \approx -2.53$). The large stress relaxation, high sensitivity of pressure to foam thickness in the 1- to 4-mm range, and nonlinear relationship all suggested unsuitability of the compressed foam disk as a means of imposing a controlled pressure on the powder bed.

A simple means was devised for applying light pressure levels to the powder bed which is insensitive to precise powder filling or compaction. This was accomplished by loading with a spring whose deflection is large in comparison to variations in the powder level. The following method was established: Powder was packed into a small glass jar as before, up to a level within the jar-neck constriction. A rubber disk was placed on top of the powder bed and then a metal disk, its surface lying below the jar top. The jar was capped with a cap drilled out to permit access to a coil spring which bore on the metal disk. The spring was compressed by enclosing the whole arrangement within a large jar so that the entire assembly could be vibrated as in step 3 of the procedure described earlier.

In order to measure the pressure applied, the sample jar (filled with powder and topped with the rubber and aluminum disks and cap) was placed

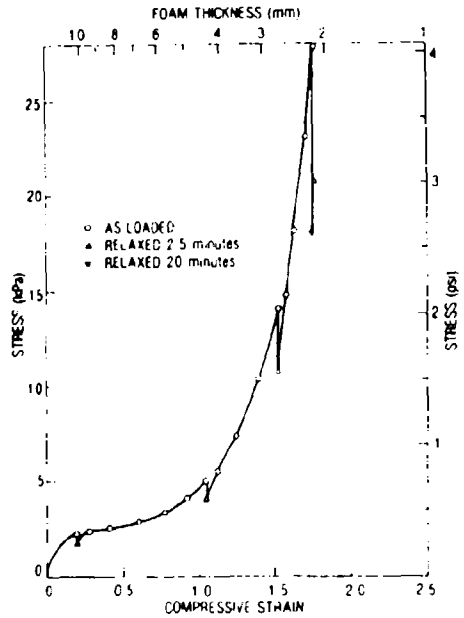

Figure 5.

Compression test results on polyurethane foam pad used to provide pressure in early packed-bed powder coating experiments.

on a common household scale which was then adjusted to zero. The inverted outer jar, with the spring attached to its bottom, was then lowered over the sample jar so that the spring passed through the drilled cap, contacting the aluminum disk. The force required to compress the spring so that the outer jar just contacted the scale platform was measured. The whole assembly was then removed from the scale, and the inverted outer jar was capped, thus compressing the spring with the same force as that just measured. Most coatings were made with a spring that provided a pressure of ~ 18 to 20 kPa (2.6 to 2.9 psi).

STEP 3. VIBRATION PERIOD

A rather gentle vibration was supplied by clamping the container to the base of a small motor (115 V, 0.90 A, 1550 rpm) with an eccentric rod attached to its shaft, the whole assembly resting on three 1.27-cm-(0.5-inch) thick polyurethane foam pads. The vibration amplitude was approximately 1 mm. Vibration times ranged from 30 to 90 minutes, to make the powder packing time (step 2) negligible by comparison.

STEP 4. LOOSE POWDER REMOVAL

The shake-out procedure made use of special tongs composed of two wire loops connected by a U-shaped wire and covered with polyester screening so as to form a pair of parallel screen-faced plattens; one of the wire loops had a short wire stub which was chucked in a "Dremel" vibratory engraving tool The sample and the powder were removed from the jar by inverting it over a container of the same powder and lightly contacting the

side of the jar with the edge of the vibrating loop. The sample, encrusted and impregnated with powder, was lifted out with plastic-padded forceps and grasped between the screen-faced plattens of the special tongs. When the vibrator was turned on, loose powder flowed out of the foam substrate's interstices in a few seconds.

STEP 5. CONSOLIDATION

Consolidation of the coating was performed by heating in an oven at about 130 ^{o}C, usually for 30 minutes. This step also delivered adhesive to the coating's outer surface in order to permit repeating the cycle of the coating process steps.

COATING EVALUATION

Visual examination under a binocular microscope at 10X was used to examine the uniformity of the coatings and the extent and nature of the defects. The amount of adhesive applied and the amount of ceramic powder incorporated into the coating in each cycle of the coating steps were monitored by weight changes. These weight changes are expressed as approximate average thickness values in order to assist in interpretation of their physical significance. The conversion from weight change to coating thickness, as monitored during the investigation and reported in the quarterly progress reports, employed a thin-film approximation and assumed all of the ceramic shrinkage to be in the thickness direction. The latter assumption permits an estimate of the fired ceramic thickness without knowledge of its green density. However, since very little of the ceramic's total shrinkage is likely to occur before decomposition of the polymer substrate, assumption of isotropic shrinkage provides a more accurate estimate of the fired ceramic thickness.

In order to permit ceramic thickness calculations based on isotropic shrinkage during firing, the green density of the coatings was estimated as the "tap density" measured by prolonged "tapping down" of a powder sample, contained in a glass graduate, until its minimum volume was attained. The tap density was measured for three ceramic powders of particular interest; for the other powders, it was taken as the average percent of the theoretical density found in the three measured powders.

ADHESIVE THICKNESS

Let t_a be the average adhesive thickness that results from adding W_a g's of adhesive, of density δ_a, to a substrate whose weight and density are W_s and δ_s, with an average fibril diameter D_s. Then

$$\Delta_a \equiv \frac{W_a}{W_s} = \left[\left(1 + \frac{2t_a}{D_s}\right)^2 - 1\right]\frac{\delta_a}{\delta_s}$$

$$t_a = \left[\sqrt{1 + \frac{\Delta_a \delta_s}{\delta_a}} - 1\right]\frac{D_s}{2} \qquad (2)$$

A PMMA-coated polyurethane foam sample, prepared in the same way as those used in this investigation, had a measured density $\delta_s = 1.158$ g/cm^3 and an average fibril diameter $D_s = 300$ μm. The adhesive's density, as reported by the manufacturer, is $\delta_a = 0.95$ g/cm^3. Hence,

$$t_a(\mu m) = 150\left[\sqrt{1 + 1.22\,\Delta_a} - 1\right] \qquad (2a)$$

For typical adhesive additions, the thickness as calculated by the thin-film approximation used for the quarterly progress reports is about 4 percent higher than that calculated by Equation 2a.

FIRED-CERAMIC THICKNESS

Let t_c be the average thickness of a ceramic coating of weight W_c and volume V_c after firing to density δ_c, and let t'_c, W'_c, V'_c, and δ'_c be its green thickness, weight, volume, and density. Let $f \equiv \delta'_c/\delta_c$ and $\Delta_c \equiv W'_c/W_s$. Then, if it is assumed that the adhesive fully permeates the ceramic coating during the consolidation step of the coating process, the inner diameter of the ceramic coating is D_s, and

$$\Delta_c \equiv \frac{W'_c}{W_s} = \left[\left(1 + \frac{2t'_c}{D_s}\right)^2 - 1\right]\frac{\delta'_c}{\delta_s}$$

$$t'_c = \left[\sqrt{1 + \frac{\Delta_c \delta_s}{\delta'_c}} - 1\right]\frac{D_s}{2}$$

For isotropic shrinkage, $\frac{t_c}{t'_c} = \left(\frac{V_c}{V'_c}\right)^{1/3} = \left(\frac{fW_c}{W'_c}\right)^{1/3}$

$$t_c = \left(\frac{fW_c}{W_c'}\right)^{1/3}\left[\sqrt{1 + \frac{\Delta_c\,\delta_s}{f\,\delta_c}} - 1\right]\frac{D_s}{2}\,. \qquad (3)$$

The average fractional "tap density", relative to the theoretical density, for the three measured powders was 51.3 percent, and for all of those powders $W_c'/W_c \approx 1$. Hence, using the average value for f,

$$t_c \approx 120\left(\frac{W_c}{W_c'}\right)^{1/3}\left[\sqrt{1 + 2.26\,\Delta_c/\delta_c} - 1\right] \qquad (3a)$$

For context, a coating thickness calculated as 25 μm by the approximation used for the quarterly progress reports would be estimated as ~ 33 μm using Equation 3a. The difference arises principally from the assumption of isotropic shrinkage in deriving Equation 3a.

COATING RESULTS: ALUMINAS AND ZIRCONIA

The following powders were used in the coating experiments (in order of their first use):

A. Excel Metallurgical Inc. "3-5 CAL" alumina, nominal 1-μm particle size, + 0.1 percent MgO (Malincrodt analytical reagent), roller-milled together for 2.75 hours in 2.5 g benzene/g powder, then air dried.

B. "Linde C" alpha-alumina, nominal 1-μm particle size.

C. Norton Company "38-900" fused alumina (electronic grade), approximately 10 μm nominal particle size.

D. Excel Metallurgical Inc. "3-5 CAL" alumina, as received.

E. 12 W/o Y_2O_3-ZrO_2 (Zirconium Corporation of America, -325 mesh, prepared from 99.9 percent Y_2O_3 and nuclear-grade ZrO_2).

F. Reynolds Metals Company "RC-HP" high-purity alumina. "Typical" analysis 99.95 percent Al_2O_3, 95 percent alpha, surface area 7 to 10 m^2/g (equivalent sphere diameter ~ 0.2 μm), median crystal size 0.5 μm.

G. Alumina "CR10" (Adolph Meller Company, lot No. 2787), surface area 8 m^2/g (equivalent sphere diameter 0.2 μm). Described as "deagglomerated".

H. Same as G but calcined 1.5 hours at 1375 °C in vacuum, then lightly ball-milled dry. Surface area 5 m^2/g (equivalent sphere diameter 0.3 μm).

Power A was prepared as a coarser-particle analog of that normally used in the preparation of General Electric's Lucalox® very high-density alumina; the MgO inhibits grain growth and thereby promotes sintering to near-theoretical density. Powders B, C, D, F and H were used to explore the aggregation behavior of alternate alumina powders, and powder E was used to test reproducibility of the results obtained in earlier experiments. Preparation of the Reynolds "RC-HP" powder (Powder F) is believed to include heavy ball milling; it is a very free-flowing powder consisting of fine aggregates.

The intent of these experiments was to define a combination of specific process procedures and powder specifications, required for the preparation of a uniform ceramic coating approximately 25-μm thick (at full density), with a minimum number of process steps. Coating defects and nonuniform or inadequate pick-up of the powder may result from deficiencies in the powder and/or one or more of the process procedures, and the proper specifications of the powder and the procedure are probably interrelated. The principal focus of the experiments was on the powder-related variables and on the light pressure supplied to the powder bed during the hypothesized adhesive diffusion step (step 3).

The quantitative results are summarized in Table 4. For reference, the coating experiments are numbered, the first two digits denoting the substrate and the third digit the cycle of the coating steps.

In coating series 01 through 07, the powder pressure was provided by the compression of a polyurethane pad. In series 01 through 05, the foam compression was not measured. It is estimated that in those coating experiments recorded as "firm" pressure the foam was compressed to ~ 4 to ~ 1 mm, producing pressures from ~ 4 to ~ 50 kPa (~ 0.6 to ~ 7 psi). In those coating experiments recorded as "light" pressure, the pressure probably ranged from ~ 2 to ~ 4 kPa (~ 0.3 to ~ 0.6 psi). In coating series 06 and 07, the pressure was estimated from the measured foam compression. In all of the subsequent coatings, the spring compression method described earlier was used to provide the powder pressure.

® Registered trademark of the General Electric Company.

Table 4

QUANTITATIVE RESULTS OF ALUMINA POWDER-COATING EXPERIMENTS

Experiment No.	Adhesive t_a, μm	Powder	Pressure kPa(psi)	Time (min)	Coating t_c, μm
011	9.4	A(1	firm(4	90	7.4
012	--	A	light	30	6.9
013	--	A(2	light	30	6.3
014	--	A	light	90	6.7
021	9.8	A(3	light	60	5.0
022	--	A(3	light	30	5.0
031	11.2	B	light	30	8.8
032	--	B	firm	30	4.0
041	12.2	C	firm	30	16.7
042	--	C(3	firm	30	12.6
051	10.3	D	light	30	10.9
052	--	D	firm	30	12.1
053	--	D	firm	30	11.7
054	--	D	firm	30	10.4
061	11.0	D	~ 50(7)	30	19.6
062	--	D	~ 30(4)	30	15.1
063	--	D	~ 30(4)	30	18.6
071	12.1	E	~ 50(7)	30	18.6
072	--	E	~ 30(4)	30	10.5
081	11.9	F	120(18)	30	20.4
091	11.7	G	18(2.6)	30	9.6
101	10.3	H	20(2.9)	30	13.5
111	12.2	D	19(2.8)	30	14.3
112	--	D	19(2.8)	30	12.5

1) Powder dried an additional 42 hours at 130 °C.
2) Powder dried an additional 18 hours at 130 °C.
3) Powder ground in glass mortar and pestle just before addition to container.
4) See text for explanation of qualitative pressure designations.

COMMENTS AND VISUAL OBSERVATIONS

Experiments 01x — Lucalox Analog (Powder A)

011. Some small spherical aggregates were observed during packing. After vibration, considerable vibration was required to discharge the packed powder from the inverted container. The coating was somewhat rough with small gaps, probably due to aggregates. It was also suspected that over-firm pressure may pack the powder so it does not feed into the interstices.

012. A lighter pressure resulted in a less firmly packed powder bed, judging by quicker discharge of the powder. The coating was still rough, and a few small gaps occurred in the interior.

013. After experiment 012, the sample was heated 19 hours at 130 °C to explore the possibility that oxidation and/or polymerization of the adhesive might "set" it so that a second dip in the heptane/S-10 solution could be used to add more adhesive. A small amount of powder was removed during this dip. The pickup remained light, so availability of the adhesive probably was not limiting.

014. The coating was somewhat rough, but appeared continuous.

Experiments 02x — Lucalox Analog (Powder A)

021. The sample interstices may have been poorly filled due to a large powder addition before tapping in. The sample had a very speckled light coating, except for an area within about 1 mm from one horizontal (in the container) face.

022. The coating was slightly rough and not quite continuous. It was thinner when viewed from one horizontal face than from the other.

Experiments 03x — Linde C (Powder B)

031. No spherical aggregates were visible to the naked eye during packing. Nevertheless, the coating was speckled, apparently due to small aggregates. The coating was almost complete near the surface, but sparser in the interior.

032. The coating appeared nominally continuous at 20X, but was composed of very small aggregates with interaggregate gaps easily visible at 140X.

Experiments 04x -- Norton 38-900 (Powder C)

041. The coverage was nonuniform but was complete in some areas of the sample. The coating was composed of small aggregates.

042. The sample was almost fully covered, but had a few small holes. The aggregates were not eliminated by grinding the powder just before its addition.

Experiments 05x — Excel "3-5 CAL" (Powder D)

051. The coverage was nonuniform; most of the area near the surface was continuous, while some small patches were very thinly coated.

052. The coating was a little bumpy, but continuous.

054. Using a "firm" packing pressure, continuing additions of ~ 10 μin/process cycle occurred.

Experiments 06x — Excel "3-5 CAL" (Powder D)

These were the first experiments made with measured compression of the foam pressure pad.

061. The near-surface coverage was complete and continuous, except for a few thin areas near the fibril junctions. The interior coverage was somewhat better than experiment 051, but patchy; the coverage density changed discontinuously at the edges of thin patches. The coating was more nearly complete when viewed from one horizontal face than from the other.

062. The sample was packed with its poorer-covered side up. The coating was a bit lumpy, but essentially complete.

063. Using "very firm" packing pressure, sustained large additions (15 to 19 μm/cycle) occurred.

Experiments 07x — Stabilized Zirconia (Powder E)

The 07x experiments were conducted to compare the coating behavior of the alumina powders with that of the "as-received" zirconia used earlier.

071. Very few spherical aggregates were observed during the powder packing procedure, but the powder seemed a bit more free-flowing than any of the aluminas tried thus far. The coating appeared fairly uniform when viewed from one horizontal face; when viewed from the other side, the sample interior was more lightly covered, with some bare areas.

072. The coating appeared generally uniform.

Experiment 081 -- Reynolds RC-HP (Powder F)

The purpose of this experiment was to determine whether the aggregates responsible for this powder's free-flowing characteristics might be broken down by the (relatively) high pressure, while its initial free-flowing characteristic would enhance the powder's penetration into the foam's interstices.

During powder loading, a few of the preformed aggregates were large enough to resist temporarily penetration into the foam; otherwise, powder appeared very free-flowing. After 30-minute vibration under this pressure, the powder was rather resistant to removal from the jar by contact with the Dremel vibrator. However, the powder flowed out of the foam interstices quite readily, except for a few loose agglomerate particles. This suggests that interparticle bridging in the bed may inhibit pressure transmission into the interior of the foam. The coating consisted of an approximate monolayer of small agglomerates, with interagglomerate gaps of comparable size. There was no evidence of agglomerate breakdown.

Experiment 091 — Meller CR10 (Powder G)

This "deagglomerated" powder had a very strong tendency to form agglomerates. During powder loading, it was necessary several times to "pour off" the agglomerates that almost covered the bed surface. In view of this characteristic, the whole spring-loaded powder bed assembly was manually tapped on the table for one minute, to promote powder penetration, before commencing the usual 30-minute mild mechanical vibration. The powder could not be removed from the jar by contact with the Dremel vibrator. Upon tapping the jar in a petri dish a large powder-cake split off, separating at the foam sample top surface. Dremel-vibration then removed the sample and most of the remaining powder. The coating coverage was poor, particularly in the interior, and the top/bottom was asymmetrical. The principal coating units were agglomerates, estimated to be ~ 50 μm (0.002 inch) in diameter.

Experiment 101 — Calcined Meller CR10 (Powder H)

The powder seemed to penetrate well during loading, with little formation of visible agglomerates. After vibration the powder unloaded readily upon contact with the Dremel vibrator. The coating coverage was speckled, with a considerable range of agglomerate sizes, up to ~ 50 μm. A few nearly bare regions were even larger, perhaps due to removal of large agglomerate particles.

Experiments 11x — Excel "3-5 CAL" (Powder D)

111. Agglomerates were visible during shake-out of the powder from the sample interstices. The coating was slightly rough (suggesting some agglomerates were involved) and had a few breaks in continuity. The coating was fairly uniform in thickness and was symmetrical.

112. This experiment followed the same procedure and had the same shake-out characteristics as experiment 111. The coating was slightly rough, and was continuous except for a few gaps very deep in the sample, as viewed from one side.

CHARACTERIZATION OF ALUMINA POWDERS

Since the Excel "3-5 CAL" alumina (powder D) seemed most nearly satisfactory of those tried, an inquiry was made to the Excel Metallurgical Company for any available information concerning it. Excel could not identify the designation on their label, so characterization efforts were initiated in our (General Electric) laboratory.

Light and electron micrographs were made of the "3-5 CAL" alumina (powder D), and electron micrographs were made of normally labeled Excel 0.3-μm and 1-μm alumina polishing powders and of the Lucalox mix (powder A) prepared by milling "3-5 CAL" with 0.1 percent MgO in benzene. The "3-5 CAL" micrographs (e.g., Figure 6) showed a rather wide range of particle sizes, with a large number of particles in the 0.5- to 1-μm range, an apparent dominance by volume of 3- to 5-μm particles, and few larger particles, up to ~ 10 μm. The particles had sharp edges and aspect ratios in the range of 1 to 2. The Lucalox mix micrographs (e.g., Figure 7) showed no particles larger than ~ 1 μm, and the particle edges were quite rounded. In addition there was a substantial amount of aggregated fines, with individual particles in the 50- to 100-Å range. The larger particles resemble those in normally labeled 1-μm polishing powder in size range and configuration (Figure 8). Aggregated fines similar to those in the Lucalox mix were found in the nominal 0.3-μm powder, but not in the 1-μm powder (compare Figures 8 and 9).

X-ray diffractometer analysis of the Lucalox mix powder indicated only alpha-alumina, as expected; but the as-received "3-5 CAL" powder had additional peaks that index as beta-alumina. This observation is quite puzzling. It would imply substantial contamination (sodium or other alkali metal), which would not be removed by the processing used to prepare the Lucalox mix. X-ray fluorescence analysis (for all elements above sodium in atomic number) indicated that the "3-5 CAL" had very small amounts of Zr, Ga, Zn, Fe, Ti, Ba, and K, and Ca in the range of 0.1 to 1 percent, all of which were absent in the Lucalox mix.

The micrographic observations suggest that "3-5 CAL" alumina may be a powder sieved to nominal 3- to 5-μm particle size, with finer particles either carried along or perhaps produced by the ultrasonic treatment used in preparing the dispersion for observation. The powder is apparently very friable, judging by the edge rounding and elimination of the larger particles after roller-milling for 2.75 hours. The differences in structural content of the "3-5 CAL" and Lucalox mix powders remain unresolved.

CONCLUSIONS FROM ALUMINA COATING EXPERIMENTS

1. Visual observations after the first-coat experiments provide a satisfactory qualitative screening test of coating uniformity. Quantitative measurements of the total coating uniformity need not be a part of this preliminary screening of powder quality.

2. The coating thickness (weight) increments on successive coating cycles provide a test of the adequacy of the adhesive.

3. For the packed-bed powder coating process, the most important characteristic of powder behavior is its tendency to form aggregates.

Figure 6. Electron micrograph of Excel "3-5 CAL" alumina (powder D). 5000X

Figure 7. Electron micrograph of Lucalox mix (powder A). 25 000X

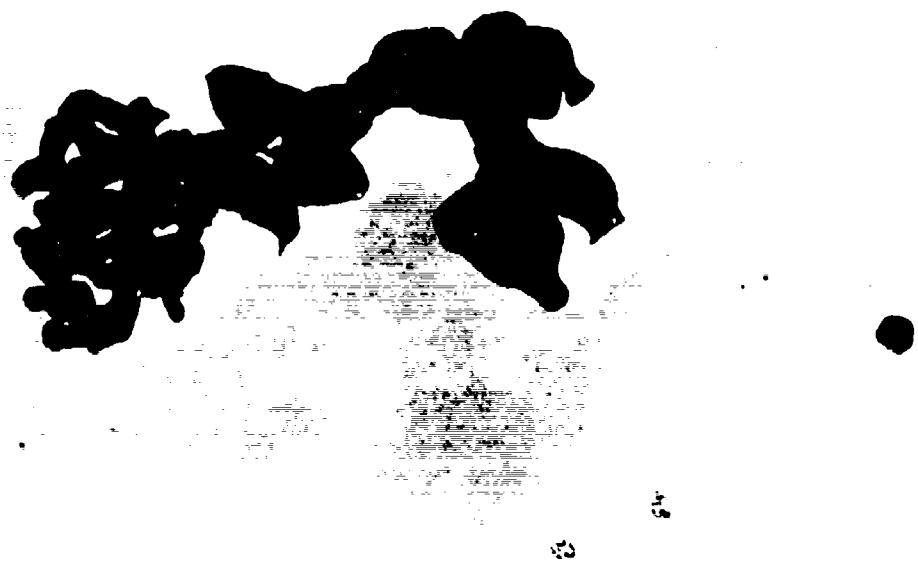

Figure 8. Electron micrograph of Excel 1-μm alumina polishing powder. 25 000X

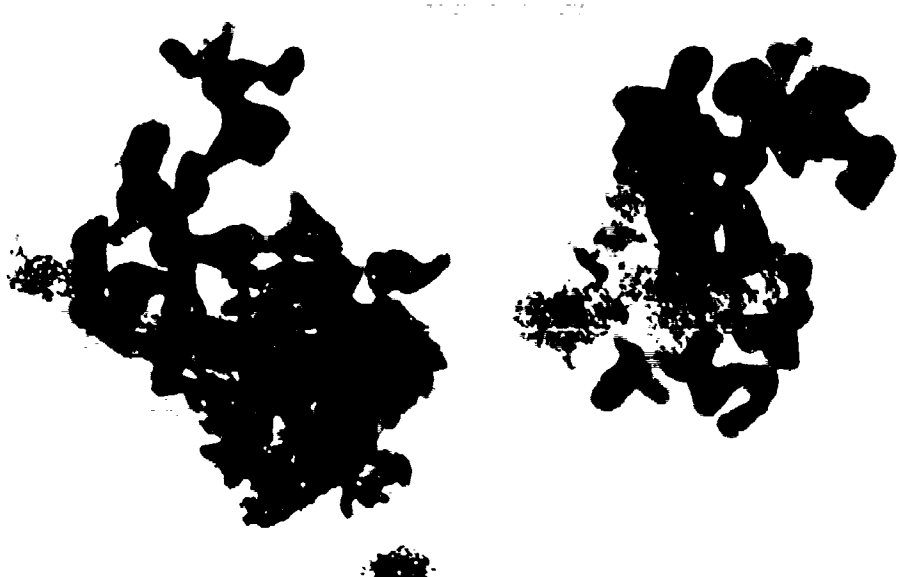

Figure 9. Electron micrograph of Excel 0.3-μm alumina polishing powder. 25 000X

4. Other variables, in addition to particle size, have substantial influence on a powder's tendency to form aggregates.

5. A powder's capability to flow into the substrate's interstices is probably related to its resistance to aggregate formation, i.e., a single "packing" property governs both.

6. Packing pressure is an important process variable and should be controlled quantitatively.

7. Adhesive thickness in the range of 9 to 12 μm appears adequate for the preparation of ceramic coatings greater than 25 μm in thickness (as-sintered).

8. Excel 3-5 alumina (powder D) is the most nearly satisfactory powder of those studied in its behavior in the packed-bed powder coating process. Its relative freedom from agglomerate formation is probably due to its coarse particle size.

"CONVENTIONAL" CERAMIC COMPOSITIONS

In view of the conclusion that only coarse particle size had provided freedom from agglomerate formation in the powders tested so far in the packed-bed powder process, it was decided to shift attention to ceramic compositions more amenable to sintering, which permit use of large particle sizes. These more "conventional" multi-component ceramics contain some liquid phase at sintering temperatures, and usually some glassy phase at lower temperatures, as distinguished from the pure oxide ceramics investigated previously. It was recognized that the presence of a glassy phase would probably increase the diffusive permeability to heat-exchange gases. However, it seemed desirable to accept this potential disadvantage at least temporarily, in the interest of improving the likelihood of quickly attaining a leak-tight microtubular structure.

The candidate ceramics considered were high-quality engineering whiteware ceramics in the Al_2O_3-MgO-SiO_2 system, such as mullite, forsterite, steatite, and cordierite ceramics. These ceramics are normally prepared from mixtures of silicate minerals rather than from the terminal oxides of the ternary system. Accordingly, experiments were conducted on packed-bed powder coating using various mineral or single-oxide powders to identify powders that might be used either singly or in combination to prepare desired compositions in the Al_2O_3-MgO-SiO_2 system. In addition, coating sequences were conducted using powder ground from a prefired foresterite ceramic, a fused synthetic forsterite powder, and feldspar, useful as a source of the fluxing agents Na_2O and K_2O.

Packed-bed powder-coating experiments were performed as generally described earlier, using the spring-loaded arrangement to maintain pressure in the powder bed. The vibration time for all of the coatings was 30 minutes. Unless otherwise noted, the spring pressure was approximately 19 kPa (2.8 psi), and the coating consolidation was 30 minutes at ~130 °C. The following powders were used (the letter identification follows that of the single-oxide powders examined earlier):

I. Calcined Kyanite

Supplier: Kyanite Mining Corporation

Typical analysis:

Al_2O_3	59.2 - 61.8 %	CaO	0.03 %
MgO	0.01	FeO	0.16 - 0.94
SiO_2	38.7	TiO_2	0.67
Alkalies	0.42		

This material is a mixture of mullite ($3Al_2O_3 \cdot 2SiO_2$) and silica. According to Professor Jesse Brown of the Virginia Polytechnic Institute, consultant to the supplier, it contains ~12 percent free silica as colloidal cristobalite, with small amounts of quartz.

The calculated theoretical density is ~3.00 g/cm^3.

J. Sierra Talc No. 1

Typical analysis:

Al_2O_3	0.7 %	CaO	8.6 %
MgO	27.8	Fe_2O_3	0.3
SiO_2	52.8	Ignition Loss	8.1
Na_2O	1.2		

The theoretical density is 2.83* g/cm^3.

*The theoretical density is not corrected for possible changes due to loss on ignition.

K. Kentucky Ball Clay

Typical analysis:

Al_2O_3	20.5 - 33.4 %	Fe_2O_3	0.9 - 1.6 %
MgO	trace - 0.51	TiO_2	0.2 - 1.9
SiO_2	51.6 - 66.2	SO_3	0.03 - 0.11
K_2O	0.28 - 1.64	P_2O_5	0.03 - 0.15
Na_2O	0.08 - 0.55	Ignition Loss	8.67 - 12.82
CaC	0.05 - 0.55		

For purposes of estimating post-firing coating thickness, the theoretical density was taken as that for kaolinite ($Al_2O_3 \cdot 2SiO_2 \cdot 2H_2O$), 2.6* g/cm^3.

L. E.P. Kaolin, Florida, Lot B

Supplier: Edgar Plastic Kaolin Company

Typical analysis:

Al_2O_3	38.26 %	PbO	0.02 %
MgO	--	Cr_2O_3	0.01
SiO_2	45.58	Fe_2O_3	0.70
K_2O	0.33	TiO_2	0.42
Li_2O	0.15	ZrO_2	0.10
Na_2O	0.11	V_2O_5	0.05
BaO	0.01	Ignition Loss	13.43
CaO	0.18		

The theoretical density was approximated as that for kaolinite, 2.6* g/cm^3.

*The theoretical density is not corrected for possible changes due to loss on ignition.

M. 38-400 Alumina

Supplier: Norton Company

Typical analysis:

Al_2O_3	99.8 %	CaO	<0.02 %
MgO	<0.02	Fe_2O_3	0.03
SiO_2	0.02	ZrO_2	<0.02
Alkalies	<0.02	C	0.034

This is a high-grade electronic grade of fused alumina, nominal 400-mesh particle size.

The theoretical density is 3.97 g/cm^3.

N. Volclay Bentonite

Typical analysis:

Al_2O_3	20.7 %	Fe_2O_3	3.03 %
MgO	2.30	TiO_2	0.14
SiO_2	64.3	P_2O_5	0.01
K_2O	0.39	SO_3	0.35
Na_2O	2.59	Other	0.01
CaO	0.52	Combined H_2O	5.14
FeO	0.46		

Bentonites are clays formed by the decomposition of volcanic glasses. The principal mineral constituent is montmorillonite, a hydrated aluminum-magnesium-sodium silicate. The density of minerals of the montmorillonite group "after dehydration by oven drying" [Ref. 7] ranges from ~2.2 to 2.7. For purposes of estimating a post-firing coating thickness, the density of bentonite has been taken as 2.5 g/cm^3.

*The theoretical density is not corrected for possible changes due to loss on ignition.

Ref. 7 R. Papin, "Bentonite", Encyclopedia of Chemical Technology, 2d edition, John Wiley & Sons, Inc., New York, Vol. 3, 1964, pp. 339-360.

O. F202 Forsterite

A prefired forsterite ceramic, reground to -325 mesh. The reported batch formulation [Ref. 8] is:

Sierramic talc	40 %
$Mg(OH)_2$	40
BaF_2	10
Kentucky ball clay No. 4	7
Bentonite	3

The theoretical density was taken as 3.15 g/cm^3, the high end of the range reported for commercial F202 forsterite ceramic.

P. No. 1736 Treasure Talc

Supplier: Whittaker, Clark & Daniels, Inc.

Typical analysis:

Al_2O_3	0.79 %	Fe_2O_3	0.11 %
MgO	33.1	P_2O_5	0.07
SiO_2	61.2	SO_3	0.01
Na_2O	0.03	Ignition Loss	4.35
CaO	0.20	Moisture Loss	none

The fired density reported by the supplier is 2.69 g/cm^3.

Q. K-200 Feldspar

Supplier: The Feldspar Corporation

Typical analysis:

Al_2O_3	18.3 %	Na_2O	3.8 %
MgO	trace	CaO	0.36
SiO_2	67.1	Fe_2O_3	0.07
K_2O	10.1	Ignition Loss	0.26

Feldspars are solid solutions of albite ($Na_2O \cdot Al_2O_3 \cdot 6SiO_2$), orthoclase ($K_2O \cdot Al_2O_3 \cdot 6SiO_2$), and anorthite ($CaO \cdot Al_2O_3 \cdot 2SiO_2$), with some free silica. Omitting impurities, the composition of K200 feldspar may be reformulated as 32.3 percent albite, 59.9

Ref. 8 L. Navias, "Advances in Ceramics Related to Electronic Tube Developments", Journal of the American Ceramic Society, Vol. 37, 1954, pp. 329-350.

percent orthoclase, 1.8 percent anorthite, 0.5 percent alumina, and 5.6 percent free silica. (The "free alumina" is probably an artifact resulting from minor analytical errors.) Based on these constituents, the calculated theoretical density is 2.57 g/cm^3.

R. C-70 Forsterite

Supplier: Muscle Shoals Electrochemical Corporation

Typical analysis:

Al_2O_3	0.2 %	CaO	0.4 %
MgO	56.6	Fe_2O_3	0.1
SiO_2	42.7		

This is a synthetic forsterite produced by melting high-purity materials in an electric arc furnace. The phase composition calculated from its nominal analysis is ~ 99 percent forsterite ($2MgO \cdot SiO_2$). The powder sample used was screened through 325 mesh. The theoretical density was taken as that for the pure compound, 3.223 g/cm^3.

S. Silica

Several silica powders were prepared, based principally on various particle sizes of Minusil (supplier: Pennsylvania Glass Sand Corporation).

Typical analysis (30 micron):

Al_2O_3	0.09 %	CaO	trace
MgO	trace	Fe_2O_3	0.023 %
SiO_2	99.90 %		

The first silica powders were prepared using 5-μm Minusil. This is a high-purity crystalline silica, ~98 percent below 5 μm, 70 percent below 2 μm in particle size. As-received, it was severely agglomerated; on screening, it immediately reformed agglomerates. An attempt to remove the fines by an alcohol wash did not improve the agglomerating tendency. Additional powders were prepared by blending 5-μm Minusil with 5 to 20 percent of Cabosil 0, a high-purity colloidal silica with a particle size of ~0.01 μm. The powder with 5 percent Cabosil still had a serious tendency to agglomerate, and very little would pass through a 325-mesh screen. Powders with 10 percent or 20 percent Cabosil, designated S_1 to S_3, were free of agglomerates and were used in the coating experiments.

S_1. 5-μm Minusil + 10 percent Cabosil 0. Roll-blended then screened through 270-mesh and 325-mesh screens.

S_2. 5-μm Minusil + 20 percent Cabosil 0. Roll-blended then screened through 60-, 170-, and 325-mesh screens.

S_3. -170 + 325 screen fraction from the preparation of S_2.

Silica powders used without Cabosil additions were:

S_4. 30-μm Minusil, ~98 percent below 30 μm, 55 percent below 10 μm in particle size.

S_5. 10-μm Minusil, ~98 percent below 10 μm, 50 percent below 3 μm in particle size.

These are high-purity crystalline silica powders. The 30-μm grade was used as-received, while the 10-μm powder was screened through a 325 mesh to break up any agglomerates in the as-received powder.

The theoretical density for all of the silica powders was taken as 2.203 g/cm^3, that of silica glass, since silica would likely be added to the powder mixtures to increase their glass-phase content.

T. No. 1 Calcined Magnesite

Supplier: Michigan Chemical Company (now the Velsicol Chemical Corporation)

Typical analysis:

Al_2O_3	0.04 - 0.20 %	CaO	0.55 - 1.00 %
MgO	97.2 - 99.0	Fe_2O_3	0.05 - 0.25
SiO_2	0.20 - 0.40	Ignition Loss	0.0 - 0.5

The theoretical density was taken as that for pure MgO, 3.576 g/cm^3.

U. "Pseudo-kaolin" Powder Mixture

This powder is a mixture of 75 percent calcined kyanite (powder I) and 25 percent Cabosil M-5, a high-purity colloidal silica. The powders were blended and screened through 270 mesh. The composition was calculated to match the alumina/silica ratio of kaolin, as a possible response to the finding that all of the fast-coating powders identified at that time were deficient in silica content compared to the clays used as the constituents of conventional ceramics.

For estimating equivalent "fired-coating thickness" from the coating weight, the theoretical density was taken as that of kaolin, 2.6 g/cm^3.

V. "Electrical Insulator" Powder Mixture

This powder is a mixture of 29 percent calcined kyanite (powder I) 34 percent feldspar (powder Q), and 37 percent 10-μm Minusil (powder S_5). This mixture corresponds in composition to the electrical insulator ceramic formulation published by Norton [Ref. 9].

All of the powders were individually screened through 325 mesh, the mixture was then weighed out and tumble-blended, and finally screened again through 325 mesh to break down any aggregates formed during the mixing operation.

The powder's theoretical density, calculated without regard for homogenization or reaction among the constituent powders, is 2.56 g/cm^3.

W. "Parian" Powder Mixture

This powder is a mixture of 28 percent calcined kyanite (powder I), 60 percent feldspar (powder Q), and 12 percent 10-μm Minusil (powder S_5). This mixture corresponds in composition to the "Parian" ceramic formulation published by Norton [Ref. 9]. The preparation procedure was the same as for powder V.

The powder's theoretical density, calculated as above, is 2.646 g/cm^3.

PACKED-BED POWDER COATING RESULTS

As for the single oxides, the coating experiments are identified by a three-digit number, the first two denoting the sequence on a particular substrate and the last digit indicating repeat coating cycles. Quantitative results of the coating experiments are summarized in Table 5.

COMMENTS AND VISUAL OBSERVATIONS

Experiments 12x — Calcined Kyanite (Powder I)

No aggregate formation was observed during the packing operations, and the powder flowed very smoothly into the foam interstices. After the first coating cycle (experiment 121), the coating appeared somewhat sparse (salt-and-pepper) and looked less fully coated in the sample interior than near its surface. After the second coating (122), the coverage was probably complete and definitely appeared complete after the third coating.

Ref. 9 F. H. Norton, Elements of Ceramics, Addison-Wesley Publishing Company, Reading, Mass., 1952.

Table 5

QUANTITATIVE RESULTS OF Al_2O_3-MgO-SiO_2 SYSTEM POWDER COATING EXPERIMENTS

Experiment No.	Adhesive t_a, μm		Powder	Coating t_c, μm
121	10.9	I.	Calcined kyanite	24.4
122	--			10.2
123[1]	--			5.5
131	10.3	J.	Sierra talc No. 1	9.2
132	--			3.7
133	--			3.9
141	9.1	K.	Kentucky ball clay	5.6
142	--			5.0
143[2]	--			2.8
144	--			2.2
151	11.4	L.	E.P. Kaolin	6.9
152	--			4.2
161	11.5	M.	38-400 Al_2O_3	23.9
162	--			7.0
163	--			5.8
171	8.8	N.	Volclay bentonite	10.9
172	--			3.8
173	--			3.5
181	10.3	O.	F-202 forsterite[3]	10.4
182	--			7.4
183	--			7.3
191	11.2	P.	Treasure talc	7.9
192	--			3.7
193	--			3.5
194	--			2.8
201	10.6	Q.	Feldspar	13.9
202	--			6.1
203	--			5.9
211	12.3	R.	C-70 forsterite	11.3
212	--			5.2
213	--			4.4
214	--			4.2
221	13.1	S_1.	Silica	< 8.2
222	--			6.9
223	--			6.7
231	7	S_2.	Silica	~ 4.6[4]
232	--			4.2
233	--			3.4
241	8.3	S_3.	Silica	4.9
242	--			3.4
243	--			3.1
251	11.0	T.	Magnesite	15.6
252	--			11.0
253	--			8.9
261	11.7	U.	Pseudo-kaolin	6.9
262	--			2.8
263	--			1.4
271	12.0	S_4.	30-μm Minusil	23.2
272	--			9.9
273	--			9.4
281	11.2	S_5.	10-μm Minusil	16.6
282	--			12.1
283	--			14.7
291	8.8	V.	"Electrical Insulator"[5]	18.4
292	--			8.0
293	--			7.3
294	--			5.4
301	8.8	W.	"Parian"[6]	20.1
302	--			8.4
303	--			5.7
304	--			6.6
311	9.5	O.	F-202 forsterite[3]	22.2
312	--			11.8
313	--			13.4

1) Follows ~19 hours at 130 °C consolidation of preceding coating layer.
2) Follows overnight at room temperature then a second 30 minutes at 130 °C to provide a "dry" initial weight. Spring pressure is 46 kPa (6.7 psi).
3) Coating thickness values calculated using measured "tap density" of 1.36 g/cm^3 as "green density."
4) Accidentally omitted weighing after application of adhesive. First-coat thickness estimated on assumption that adhesive weight corresponded to average adhesive thickness of prior experiments (11.0 μm).
5) As above, tap density is 1.51 g/cm^3.
6) As above, tap density is 1.38 g/cm^3.

Experiments 13x -- Sierra Talc No. 1 (Powder J)

No aggregate formation was observed during packing. The powder flowed so easily that it readily rose around the edges of the rubber disk normally used to close off the top of the powder bed. A thin rubber membrane, extending between the jar threads and the cap, was placed between the rubber disk and the aluminum disk to assure that the spring pressure applied to the powder bed would not cause continued outflow of the powder. The presence of this membrane may reduce somewhat the pressure delivered to the powder bed.

After the first coating (131), the coating appeared sparse (salt-and-pepper) but uniformly throughout the sample. It appeared to be uniform and fully covered after the second coating (132).

Experiments 14x — Kentucky Ball Clay (Powder K)

This powder filled very smoothly, again with no aggregate formation, and appeared to need a rubber membrane to assure containment of the powder. The coating appeared essentially complete (little salt-and-pepper) after the first coating (141). Increased pressure applied during the third coating step had little, if any, value in increasing the coating thickness per cycle.

Experiments 15x — E. P. Kaolin (Powder L)

Occasional small aggregates were formed during the packing operation. For the first coating sequence, a rubber membrane was again used to assure containment of the powder, but was omitted in the second cycle. After both the first and second coating steps, a few completely bare areas were observed on the substrate. These bare patches resembled those encountered in earlier (precontract) work, apparently due to spalling off of the coating, with its associated adhesive, during the powder shake-out step. This defect appeared to be associated with excessive adhesive thickness.

Experiments 16x — 38-400 Alumina (Powder M)

This powder packed in smoothly, with no visible aggregate formation. The coating had a salt-and-pepper appearance after the first coating step (161), but appeared uniform and continuous after subsequent coatings.

Experiments 17x — Volclay Bentonite (Powder N)

This powder packed in smoothly with no visible aggregate formation. Microscopic examination of the coating after the first sequence (171) indicated the presence of some aggregates, estimated to be 20 to 40 μm in diameter. The coating appeared uniform throughout the sample, and continuous after the second sequence (172).

Experiments 18x — F-202 Forsterite (Powder O)

A few aggregates were visible during the process of packing powder through the foam, but disappeared as the bed was "tapped in". A few aggregates were again observed during removal of the unbonded powder from the foam interstices. Visual observation after the first coating operation showed an incomplete or thinner (salt-and-pepper) coating in some areas, predominantly at the concave-curvature positions where the foam fibrils meet (crotches). After the second coating sequence (182), the coating was visually complete and uniform.

Experiments 19x — Treasure Talc (Powder P)

The powder packed in smoothly with no visible aggregate formation. The coating appeared uniform, but still not quite continuous after the second coating sequence (192). After the third and fourth sequences, it appeared uniform, smooth, and continuous.

Experiments 20x — Feldspar (Powder Q)

The coating was fairly complete, but had a slight salt-and-pepper appearance, uniformly distributed, after the first coating cycle (201). The coating appeared continuous after the second cycle.

Experiments 21x — C-70 Forsterite (Powder R)

After the first coating cycle (211), the coating appeared uniform but slightly salt-and-pepper, which normally indicated a noncontinuous coating. When there was no change in coating appearance after the second coating cycle (212), a bit of powder was compacted with a spatula and examined visually. It contained black particles, probably due to iron contamination.

Experiments 22x — Silica (Powder S_1)

The powder was very free-flowing, with no visible aggregate formation during the first coating cycle (221). On removal of the powder bed from the vibrator, it was found that the pressure disks had been pushed down several millimeters, and powder had flowed around their edges. The usual Dremel vibrator operation, to free powder from the interstices of the coated foam sample, failed to remove the powder packed into a few near-surface cells. (Hence, the weight gain over-estimates the average coating thickness.) Visual observation revealed a heavy coating near the sample's surface, with incomplete coating (salt-and-pepper appearance) in the sample interior.

A few agglomerates were observed during packing for the second coating cycle. A rubber membrane was placed over the upper pressure disk to

restrict the flow of powder around the disk edges. Nevertheless, the powder compacted during the 30-minute vibration period so that the disks moved inward ~5 to 6 mm, and the spring load was reduced from its usual initial value to ~14 kPa (2.0 psi). The coating now appeared continuous throughout the sample, but was rough, as associated with self-packing of the powder. The near-surface foam cells that were powder filled after the first coating cycle remained filled after the second and third cycles. In the third cycle, again using a rubber membrane over the pressure disks, the disks moved inward ~3 mm, with a pressure drop to ~17 kPa (2.4 psi).

Experiments 23x — Silica (Powder S_2)

The powder was very free-flowing; a rubber membrane was placed over the pressure disks in all of the coating cycles. Pressure drops occurred, as tabulated below.

Cycle	Initial Pressure	Final Pressure
231	17 kPa (2.4 psi)	13 kPa (1.9 psi)
232	15 2.1	14 2.0
233	16 2.3	14 2.0

The low initial pressures suggested that a significant compaction of the powder took place immediately upon spring loading.

After the first coating cycle, the coating appeared slightly salt-and-pepper, but nearly continuous, and was uniform throughout the sample. No bulk-packing of the foam cells occurred. A few agglomerates were observed in the powder that had flowed around the disk edges, and hence was not under pressure during the vibration.

After the second coating cycle, the coating appeared continuous.

Experiments 24x — Silica (Powder S_3)

This coarser sieve-fraction powder was tried in order to assess whether a thicker coating per cycle might result from adhering slightly larger aggregates. The powder was quite free-flowing, and a rubber membrane was placed over the pressure disks to limit its flow. The initial pressure for all of the cycles was a normal 19 kPa (2.7 psi) and did not change perceptibly during the vibration period of the first or third cycles. In the second cycle, it dropped to 16 kPa (2.3 psi).

After the first coating cycle, the coating was quite salt-and-pepper and consisted of ~40-μm aggregates. After the second cycle, the coating was

nearly continuous, with occasional gaps. After the third cycle, there were still a few dubious spots, particularly at the concave surfaces near the crotches where four fibrils meet. The coating was somewhat rough.

Experiments 25x — Calcined Magnesite (Powder T)

The powder flowed smoothly, but was not so free-flowing as to require a membrane over the pressure disks. The spring pressure was normal. and unchanged during vibration. After the first cycle, the coating was continuous along the foam fibrils, but thin in the neighborhood of the crotches The coating was continuous everywhere following the second cycle.

Experiments 26x — Pseudo-Kaolin (Powder U)

During the procedure of packing the foam sample into this powder the powder displayed a marked tendency to stick on the spatula used for loading it, but seemed quite free-flowing as it penetrated the foam interstices or flowed up around the pressure disk. A rubber membrane was used over the pressure disk to restrict the powder flow. During the 30-minute vibration period of the first and second coating cycles, the pressure dropped from its initial value of ~18 kPa (2.6 psi) to ~15 kPa (2.1 psi) while in the third cycle it apparently increased from ~15 kPa (2.2 psi) to ~16 kPa (2.5 psi).

After the first cycle, the coating appeared continuous near the sample surface, but uniformly salt-and-pepper in the interior Aggregates of ~10 μm in diameter were visible in the coating. After the second cycle, the coating was continuous except for a few small bare spots in the interior Some of these remained after the third cycle.

Experiments 27x — 30-μm Minusil (Powder S_4)

The powder contained some soft aggregates which appeared to disintegrate during tapping-in the bed. The pressure remained constant at ~20 kPa (2.9 psi) in all three coating cycles. After the vibration period, small aggregates were visible in the powder being removed from the foam interstices. After the first coating cycle, there were many bare or thinly coated areas on the concave surfaces near the fibril crotches in the foam interior. After the second cycle, the coating was still not quite continuous in these regions, but was continuous after the third cycle.

Experiments 28x — 10-μm Minusil (Powder S_5)

The pressure remained constant at ~20 kPa (2.9 psi) in all three coating cycles. Small aggregates were visible in the powder being removed from the foam interstices after the vibration period. After the first coating cycle, a considerable fraction of the interior was sparsely coated, particularly near the fibril crotches. After the second and third coating cycles, the coating was continuous.

Experiments 29x -- "Electrical Insulator" (Powder V)

The powder packed in smoothly with no visible aggregates, but some small aggregates were observed during removal of unbonded powder from the foam interstices. The pressure remained constant at ~ 20 kPa (2.9 psi) during all of the coating cycles. After the first coating cycle, the coating was discontinuous, and nonuniformly so, in the foam's interior. Thin spots were not particularly associated with the fibril crotches or other configurational features. In addition, there was a macrononuniformity from the top to the bottom of the foam, with the (probably) lower third of the sample more lightly coated. The second coating cycle was conducted with this lightly coated portion down, and it remained thin. The third and fourth cycles were conducted with the sample inverted, and its appearance became macroscopically uniform. After the third cycle, the coating appeared continuous, as observed from the original thinly coated side of the foam.

Experiments 30x -- "Parian" (Powder W)

The powder packed in smoothly with no visible aggregates, but some very small aggregates were observed during vibration removal of the unbonded powder from the foam interstices. The pressure remained constant at ~ 20 kPa (2.9 psi) during all of the coating cycles. After the first coating cycle, the coating was patchy with thin-to-bare areas particularly (but not exclusively) in the fibril crotches. After the second cycle, the coating was almost continuous with very few thin spots. The coating appeared continuous after the third coating cycle.

Experiments 31x -- F-202 Forsterite (Powder O)

This coating was made to prepare a sample for firing to a microtubular ceramic structure A few small agglomerates were observed during "tapping in" of the foam in the packed powder bed. After the first coating cycle, there were some thinly coated areas at the fibril crotches. The coating appeared continuous after the second coating cycle. The reason for higher coating pickups in this series, compared to earlier coatings (series 18x) with the same powder, has not been established.

CHARACTERIZATION OF SELECTED POWDERS

Electron micrographs were prepared of powders I through O, Q, S_5, and the powder mixtures V and W. The powders were ultrasonically dispersed in distilled acetone for 15 minutes, the dispersions were deposited on a carbon substrate supported by a 200-mesh copper grid, and micrographs were made on a Siemens Elmiskop 101 electron microscope at 125 kV. Magnifications were 6000X to 150 000X. The particles of the clay-type powders (kaolin, Kentucky ball clay, and bentonite) and of Sierra talc are very thin platelets, partially electron transparent. It is often impossible to distin-

guish between the discontinuities in platelet thickness and the overlap of two or more aggregated platelets. Similarly, for the K-200 feldspar, the 10-μm Minusil, and the powder mixtures "electrical insulator" and "Parian", particle overlaps and the wide range of particle sizes made quantitative measurements difficult. Hence, while the micrographs of these powders provide a qualitative indiction of their ultimate particle size, no quantitative measurements were attempted. Typical photomicrographs are provided in Figures 10 through 16.

For the calcined kyanite, the 38-400 alumina, and the F-202 forsterite, chord lengths were measured using a randomly positioned line grid; and the mean lineal traverse $\bar{l}$, the standard deviation σ_l, and the standard deviation of the mean $\sigma_{\bar{l}}$ were calculated. σ_l provides a general indication of the size dispersion, but contains also the dispersion resulting from random position and orientation of the measured chords. For context, the calculated value of σ_l for a uniform array of circular particles is ~ 0.22 $\bar{l}$. The results of these measurements are summarized in Table 6, and typical photomicrographs are provided in Figures 17 through 20.

Figure 10. Electron micrograph of E.P. Kaolin (powder L) 25 000X

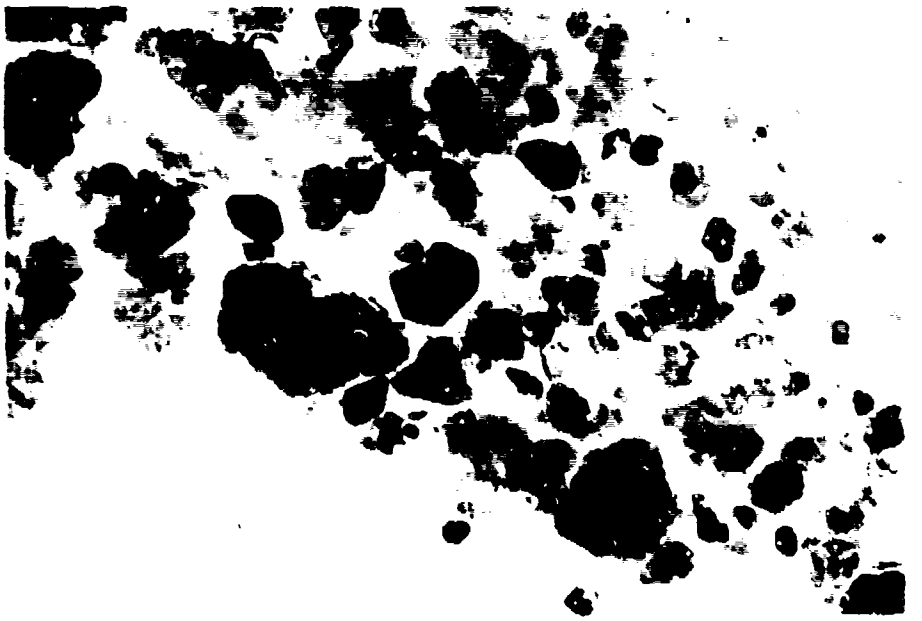

Figure 11. Electron micrograph of Kentucky ball clay (powder K) 25 000X

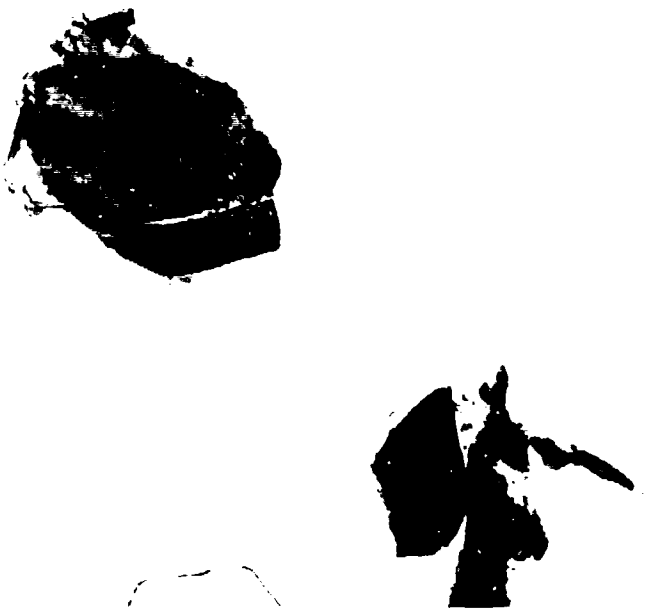

Figure 12. Electron micrograph of Volclay bentonite (powder N) 25 000X

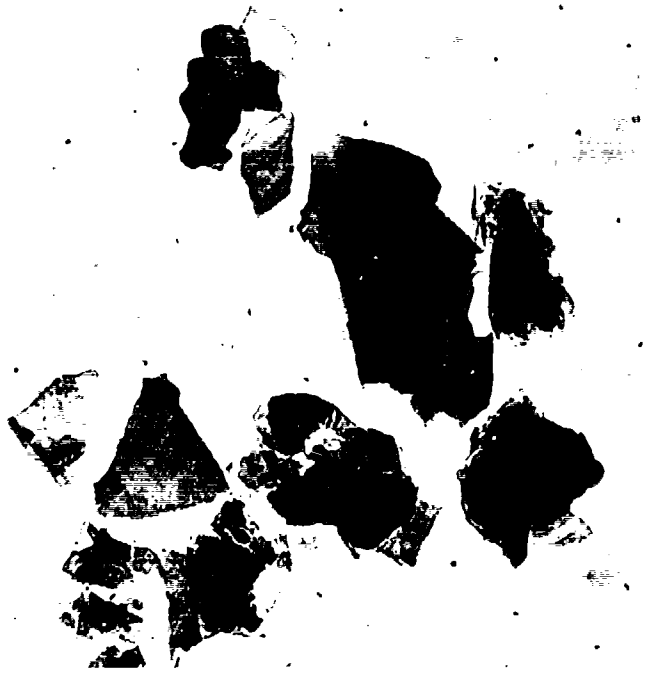

Figure 13. Electron micrograph of Sierra talc No. 1 (powder J) 25 000X

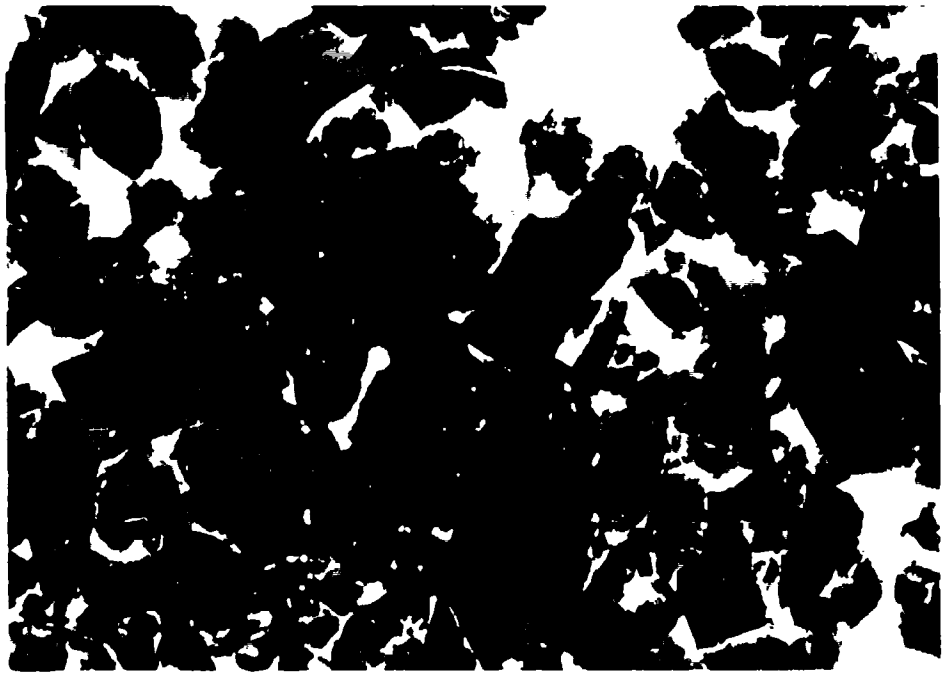

Figure 14. Electron micrograph of K-200 feldspar (powder Q) 15 000X

Figure 15. Electron micrograph of 10-μm Minusil (powder S_5) 15 000X

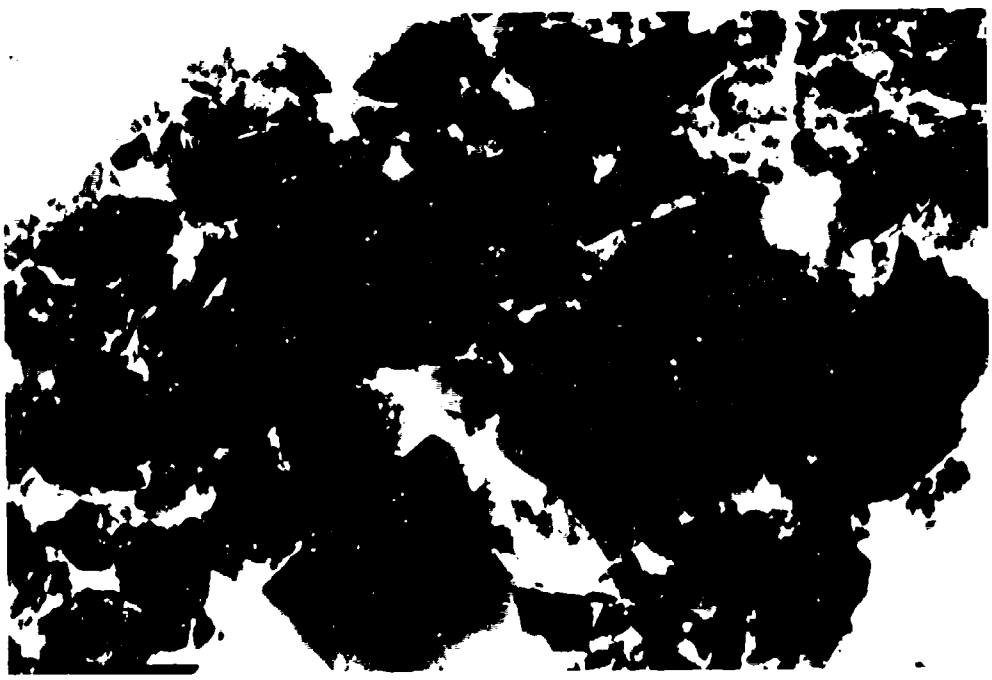

Figure 16. Electron micrograph of "electrical insulator" powder mixture (powder V) 15 000X

Figure 17. Electron micrograph of "Parian" powder mixture (powder W) 15 000X

Figure 18. Electron micrograph of calcined kyanite (powder I) 25 000X

Figure 19. Electron micrograph of 38-400 alumina (powder M) 25 000X

Figure 20. Electron micrograph of F-202 forsterite (powder O) 5000X

Table 6

PARTICLE SIZE MEASUREMENTS ON SELECTED POWDERS

		Number of Traverses		
	$\bar{l}$	N	$\sigma_l/\bar{l}$	$\sigma_{\bar{l}}/\bar{l}$
Calcined Kyanite	0.32μm	79	0.84	0.095
38-400 Alumina	0.16μm	94	0.91	0.094
F-202 Forsterite	1.39μm	76	0.95	0.109

REFORMULATION OF CERAMIC COMPOSITIONS

Table 7 summarizes the quantitative information obtained for selecting powders to prepare ceramics in the Al_2O_3-MgO-SiO_2 system by packed-bed powder coating. Approximate compositions, corrected for loss on ignition, are arranged in descending order of Al_2O_3 or MgO content for the essentially

Table 7

SUMMARY OF QUANTITATIVE INFORMATION ON Al_2O_3-MgO-SiO_2 SYSTEM POWDER COATING

	Powder	Al_2O_3	MgO	SiO_2	Alkali[1]	Other	$\bar{t}_{1-3}$ μm
M.	38-400 Alumina	100	--	--	--	--	36.6
I.	Calcined Kyanite	~60	--	39	0.4	1	40.1
L.	E.P. Kaolin	44	--	53	0.7	2	≤15.4
K.	Kentucky Ball Clay	30	--	66	1.4	3	11.5
N.	Volclay Bentonite	22	2	68	3.1	5	18.2
Q.	Feldspar	18	--	67	13.9	--	25.9
T.	Calcined Magnesite	--	99	--	--	1	35.5
R.	C-70 Forsterite	--	57	43	--	--	20.7
O.	F-202 Forsterite	4	48	36	0.9	11[2]	25.1
P.	Treasure Talc	1	35	64	--	--	15.1
J.	Sierra Talc No. 1	1	30	57	1.3	11[3]	16.8
S_5.	Silica	--	--	100	--	--	43.4

1) Sum of Na_2O, K_2O, and Li_2O content.
2) Principally BaO.
3) Principally CaO.

aluminum silicate and magnesium silicate powders, respectively, and the best-coating silica powder. Also shown, in the right-hand column, is the average coating thickness resulting from three cycles of packed-bed powder coating.

An inspection of Table 7 provides several guidelines concerning the options for formulating Al_2O_3-MgO-SiO_2 ceramics using powders most likely to be effective in the packed-bed powder coating process:

1. Feldspar is the only powder investigated that will contribute substantial amounts of the alkali oxides which increase fluidity of the glass phase and lower firing temperatures.

2. The more rapid-coating powders (alumina, kyanite, and magnesite) contain less silica than the clays and talcs commonly used as sources of alumina and magnesia in ceramic formulations. The silica powders first investigated coated very slowly (hence the trial of powder U, "pseudo-kaolin"), but powder S_5 (10-μm Minusil) coats well and can be used to compensate for the low silica content of other rapid-coating powders.

3. If the clay minerals are omitted from ceramic formulations, their alumina content may be provided by substituting either calcined kyanite or pure alumina. Kyanite would seem preferable in the interests of greater initial homogeneity.

4. If the talc minerals are omitted from ceramic formulations, their magnesia content may be provided by substituting either forsterite or pure calcined magnesite. Forsterite would seem preferable in the interests of greater initial homogeneity.

In order to permit simple reformulation of ceramic compositions in accordance with these guidelines, it is convenient to idealize the powder compositions, considering feldspar the only source of alkali oxides, omitting other minor constituents, and utilizing only the simpler forsterite (C-70, powder R) and talc (Treasure, powder P) compositions. The resulting idealized compositions are summarized in Table 8.

The reformulation equations are derived assuming that the original formulations involve only the constituents listed in Table 8, not including forsterite. Using the letter designations of the powders, with subscripts 1 and 2 to designate the original and reformulated compositions, the guidelines for reformulation may be summarized as:

$$L_2 = K_2 = N_2 = P_2 = 0$$

Table 8

IDEALIZED COMPOSITIONS OF SELECTED POWDERS

	Powder	Al_2O_3	MgO	SiO_2	Alkali
M.	38-400 Alumina	100	--	--	--
I.	Calcined Kyanite	61	--	39	--
L.	E.P. Kaolin	45.6	--	54.4	--
K.	Kentucky Ball Clay	31.4	--	68.6	--
N.	Volclay Bentonite	23.7	2.6	73.7	--
Q.	Feldspar	18.4	--	67.6	14.0
T.	Calcined Magnesite	--	100	--	--
R.	C-70 Forsterite	--	56.6	42.7	--
P.	Treasure Talc	0.8	34.8	64.4	--
S.	Silica	--	--	100	--

$M_2 = T_2 = 0$ if possible

Since only feldspar is presumed to provide alkali oxides,

$$Q_2 = Q_1 . \tag{4}$$

Since, if possible, only forsterite provides magnesia,

$$0.566\, R_2 = T_1 + 0.348\, P_1 + 0.026\, N_1$$

$$R_2 = 1.77\, T_1 + 0.615\, P_1 + 0.046\, N_1 . \tag{5}$$

Since, if possible, calcined kyanite must supply the balance of the alumina not provided by feldspar,

$$0.61\, I_2 = 0.61\, I_1 + M_1 + 0.456\, L_1 + 0.314\, K_1 + 0.237\, N_1 + 0.008\, P_1$$

$$I_2 = I_1 + 1.64\, M_1 + 0.748\, L_1 + 0.515\, K_1 + 0.389\, N_1 + 0.013\, P_1 \tag{6}$$

Finally, silica powder must supply the silica content not already furnished by calcined kyanite, feldspar, and forsterite.

$$S_2 + 0.39\,I_2 + 0.427\,R_2 = S_1 + 0.39\,I_1 + 0.544\,L_1 + 0.686\,K_1 + 0.737\,N_1 + 0.644\,P_1$$

$$S_2 = S_1 + 0.39\,(I_1 - I_2) - 0.427\,R_2 + 0.544\,L_1 + 0.686\,K_1 + 0.737\,N_1 + 0.644\,P_1 \,. \qquad (7)$$

Tables 9 and 10 illustrate numerically the application of the reformulation equations. Table 9 reproduces the constituents suggested by Norton [Ref. 9] and Kingery [Ref. 10] for a number of Al_2O_3-MgO-SiO_2 based ceramics, together with the suggested firing temperatures. Table 10 lists the calculated alternate formulations with approximately the same chemical compositions but prepared only from calcined kyanite, feldspar, forsterite, and silica.

Table 9

CONSTITUENTS USED IN FORMULATING SOME TYPICAL Al_2O_3-MgO-SiO_2 SYSTEM CERAMICS

Ceramic	Kaolin	Ball Clay	Feldspar	Flint	Talc	Kyanite	Firing Temperature Cone	Firing Temperature °C
Norton [Ref. 9]								
Vitreous Sanitary	28	20	32	20			12	1310
Electrical Insulator	21	25	34	20			12	1310
Will Tile-vitreous	27	29	33	11			10	1260
Semivitreous Whiteware	24	28	13	35			9	1250
Parian	30	10	60				8	1225
Hard Porcelain	35	15	25	25			16	1450
Talc Body No. 1	18		7		75		12	1310
Talc Body No. 2	18	15	35	25	7		5	1180
Dental Porcelain	5		81	14			10	1260
Refractory Porcelain	50	10	10	5		25	20	1520
Kingery [Ref. 10]								
Hard Porcelain	40	10	25	25			16	1450
Electrical Insulator No. 1	27	14	26	33			14	1390
Electrical Insulator No. 2	23	25	34	18			12	1310
Vitreous Tile	26	30	32	12			10	1260
Dental Porcelain	5		95				10	1260
Electrical Insulation	28	10	35	25	2		9	1250

Ref. 10 W. D. Kingery, Introduction to Ceramics, John Wiley & Sons, New York, 1960.

Table 10

CALCULATED ALTERNATE FORMULATIONS OF Al_2O_3-MgO-SiO_2 SYSTEM CERAMICS, EMPLOYING FAVORABLE MATERIALS FOR PACKED-BED POWDER COATING

Ceramic	Calcined Kyanite	Feldspar	Forsterite	Silica
Norton [Ref. 9]				
Vitreous Sanitary	31	32		37
Electrical Insulator	29	34		37
Wall Tile-vitreous	35	33		32
Semivitreous Whiteware	32	13		55
Parian	28	60		12
Hard Porcelain	34	25		41
Talc Body No. 1	14	7	46	33
Talc Body No. 2	21	35	4	40
Dental Porcelain	4	81		15
Refractory Porcelain	67	10		23
Kingery [Ref. 10]				
Hard Porcelain	35	25		40
Electrical Insulator No. 1	27	26		47
Electrical Insulator No. 2	30	34		36
Vitreous Tile	35	32		33
Dental Porcelain	4	95		1
Electrical Insulation	26	35	1	38

POWDER COATING CONCLUSIONS

Probably all of the mineral powders tested are suitable for use, at least as minor constituents, in a powder mixture to be coated onto foam substrates

by the packed-bed powder coating process. Calcined kyanite, K-200 feldspar, C-70 and F-202 forsterites, 10-μm Minusil, calcined magnesite, and 38-400 alumina all coat rapidly enough to be candidate major constituents, although 38-400 alumina may be rather coarse compared to desired microtube dimensions. All of the clays and talcs tested coated rather slowly suggesting they be restricted to possible use as minor constituents. Experiments in which minor additions of cabosil were used to prevent or reduce agglomerating tendencies of other powders led to thin coatings. Thus, this material appears unsuitable for use in the process, even as a minor constituent.

A wide variety of ceramic compositions in the Al_2O_3-MgO-SiO_2 system can in fact be reformulated for preparation using only fast-coating powders. Coatings made with two such mixtures demonstrated qualitatively that the desirable coating behavior of individual powders carries over into mixtures prepared from them.

The mechanism of the packed-bed powder coating process was not investigated as a part of this study, nor were the process variables extensively studied. However, observations made during the study suggest features that were not included in the hypothesized model originally used to establish the process procedure. The salt-and-pepper appearance of thin coatings, characteristic of the first coating cycles of even fast-coating powders, suggests that the coating mechanism is predominantly single-layer adhesion of small aggregates rather than multilayer accretion of individual powder particles by permeation of the adhesive. If so, the hold time between embedding the substrate and removing the nonadhering powder may be unimportant.

Quantitative tap-density measurements on three powders*, made only after most of the powder coating experiments had been concluded, indicated that, for those powders, more "tapping time" was required to achieve maximum tap density than characterized the usual preparation of a packed powder bed encompassing a foam substrate. This observation suggests a speculation, that the powder bed's green density may be an important variable, which was not monitored during this study. The possible importance of tap density as a process variable would be consistent with the earlier finding of the significance of applied pressure. Differences in the duration of tapping, and hence of green density, might be responsible for the heavier F-202 forsterite coatings produced in the 31x series of coating experiments, compared to those of the 18x series. The later experiments were conducted following the tap-density measurements, and preparation of the powder beds was influenced by awareness of the time required to achieve maximum density.

*Tap-density measurements were made on F-202 forsterite (powder O), and the powder mixtures "electrical insulator" (powder V) and "Parian" (powder W).

Section 5

FIRING EXPERIMENTS

PROCEDURES

Firings were performed in air, unless otherwise noted. The samples were slowly heated and cooled, in the furnace, and normally were held at the designated temperature for one hour.

Approximate densities were determined from weight and dimensional measurements, and immersion density measurements were made when higher accuracy was desired. For these measurements, a small wire rack held the sample with its major surfaces inclined, to avoid trapping of bubbles. In order to minimize surface tension effects, the rack was suspended by a 43-μm (0.0017-inch) wire, and a few drops of soap solution were added to the distilled water used as the immersion fluid.

The immersed weights were reproducible to $\pm$0.1 mg, corresponding to a volume uncertainty of ~0.01 percent for the sample sizes employed. In calculating the sample densities, the density of water was corrected for temperature and the effect of the soap solution addition was checked by weighing a carefully measured volume of the immersion liquid.

Before the immersion density measurement, the samples were checked for open porosity by determining if there was a significant weight gain resulting from a 5-minute soak in distilled water. If so, the following lacquer-sealing procedure was used: The sample was lacquered repeatedly, with a solution of polystyrene in toluene, until its surface displayed a uniform glaze and there was no weight gain after a 5-minute water soak. The polystyrene's volume was calculated from the weight gain due to lacquering, and the lacquered sample's volume was determined from the difference between its weight in air and in water. The original sample macroscopic volume could then be calculated assuming: a) all of the lacquer volume is outside the sample's original volume — a minimum estimate of the sample's volume, leading to a maximum estimate of its density; or b) all of the lacquer volume has entered the surface pores and lies within the sample's original volume — a maximum estimate of the sample's volume, leading to a minimum estimate of its density.

As initially lacquered to a uniform luster and no weight gain on water soaking, the maximum and minimum estimates were unacceptably divergent. Excess lacquer could now be removed, by brushing a little toluene on the surface and wiping off the softened surface, without opening up the surface to interior open porosity. Lacquer removal was repeated if necessary and, with few exceptions, the apparent density values calculated using the two assumptions finally agreed within ~1 percent.

Very late in the contract period, a more precise method was devised for measuring the immersion density of samples with open porosity. Instead of using lacquer to seal the sample surfaces, the weight gain after a 5-minute soak in distilled water was used as a quantitative measure of open porosity and was included in the calculation of the immersion density. This method was applied only to the F-202 forsterite samples.

RESULTS

In order to provide a first test of whether aluminum silicate-type ceramics could be sintered into microtubular ceramics, without slumping or other unidentified difficulties, the foam sample coated with calcined kyanite (12x series) was fired for one hour at 1600 °C in air. No slumping nor other unusual behavior occurred. The resulting microtubular ceramic was ground against a coarse stainless steel screen to prepare chips, which were embedded in plastic and polished for microscopic examination. The observed density was very low -- clearly lower than that of pressed samples (see below). No quantitative measurements were made.

In order to investigate the effect of firing temperature on sintering without using additional microtubular samples, and to permit estimating the fired density, pressed samples of calcined kyanite were fired in air along with loose as-received powder contained in a platinum crucible. The pressed samples were prepared at 69 MPa (10 000 psi) from both as-received powder and powder ball-milled to a finer particle size. It was reasoned that the sintering behavior of microtubular ceramics prepared by the packed-bed powder coating process should lie somewhere between that of pressed samples and of loose powder, probably closer to the latter.

The first firing was done at 1700 °C for one hour. After firing, the loose powder sample had shrunk away from the crucible walls and was a nearly cylindrical free-standing body. However, it displayed macroscopic voids along its sides, resembling those visible on the sides of a sample of loose powder poured into a glass jar. Measurements of the weights and dimensions of these samples indicated densities of ~62, 93, and 94 percent of the estimated theoretical density for the as-received powder, loose and pressed, and the ball-milled-and-pressed sample, respectively.

The second firing experiment of this general type was for one hour at 1600 °C, as used for the microtubular ceramic. In this experiment, the unpressed powder was brought to "tap density" before firing, simulating its treatment in the packed-bed powder coating process. Measurements of the weight and dimensions of these samples indicated densities of ~69, 80, and 86 percent of the estimated theoretical density for the as-received powder, initially tap-dense or pressed, and the ball-milled-and pressed sample, respectively.

Figure 21 shows the microstructure of the kyanite microtubular ceramic chips, and Figures 22 and 23 show those of the loose (or tap-dense) powder and the pressed kyanite samples fired at 1600 and 1700 °C. The results of these initial firing experiments indicated that considerably higher liquid content and/or fluidity would be required to densify ceramics prepared by packed-bed powder coating than is required for the same material with higher green density, for example, as provided by pressing. No further firing experiments were done on calcined kyanite alone.

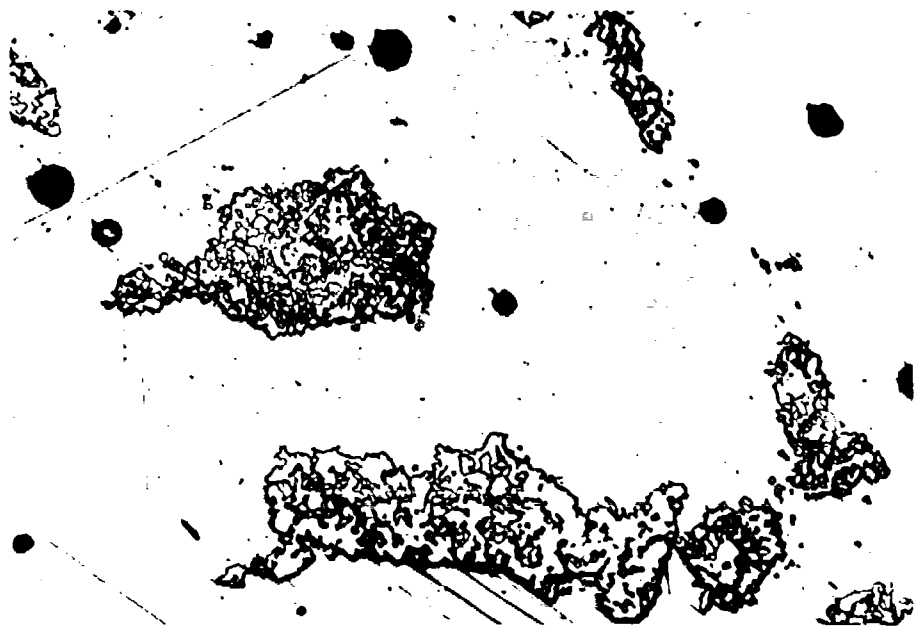

Figure 21. Chips from calcined kyanite microtubular ceramic sintered one hour at 1600 °C (75X)

Additional firing experiments were performed on the F-202 (powder O) and C-70 (powder R) forsterite powders and on the "electrical insulator" (powder V) and "Parian" (powder W) powder mixtures. Results of the density measurements after firing both pressed and tap-dense samples of these powders are summarized in Table 11. When more than one sample was measured, the density range given is from the lowest "minimum density" to the highest "maximum density" value, if the lacquered sample immersion technique was used. The F-202 forsterite, "electrical insulator", and "Parian" powder mixtures all could be fired to densities exceeding 90 percent of their theoretical density values, and showed no appreciable weight gain after immersion in water for 5 minutes. For the initially tap-dense samples, firing temperatures of 75 to 100 °C above the nominal "maturing temperature" were required, but the density of these samples then matched or exceeded that of the pressed samples fired at the same temperature.

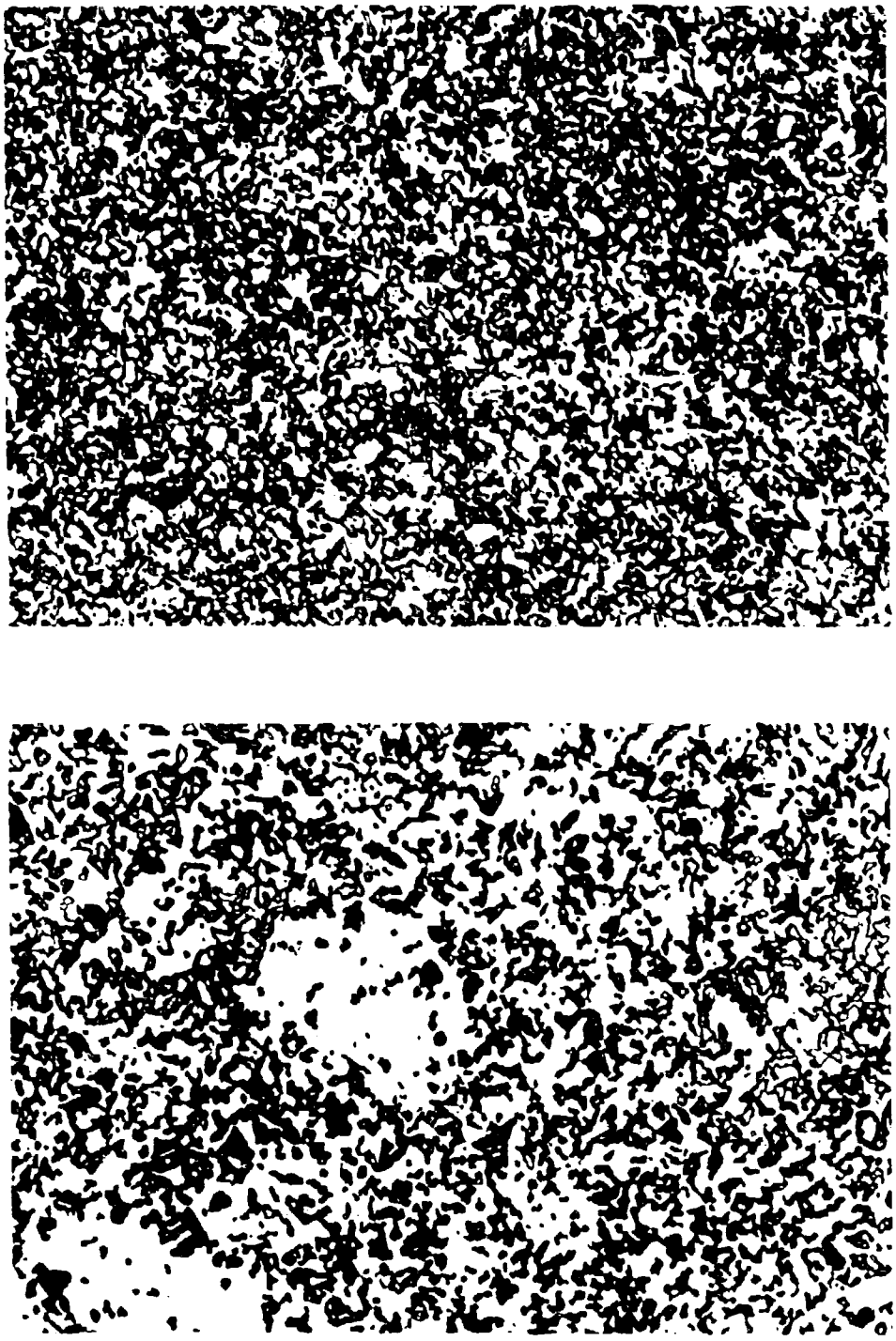

Figure 22. Sintered calcined kyanite: a) tap-dense, then fired at 1600 °C; and b) loose powder, fired at 1700 °C (75X)

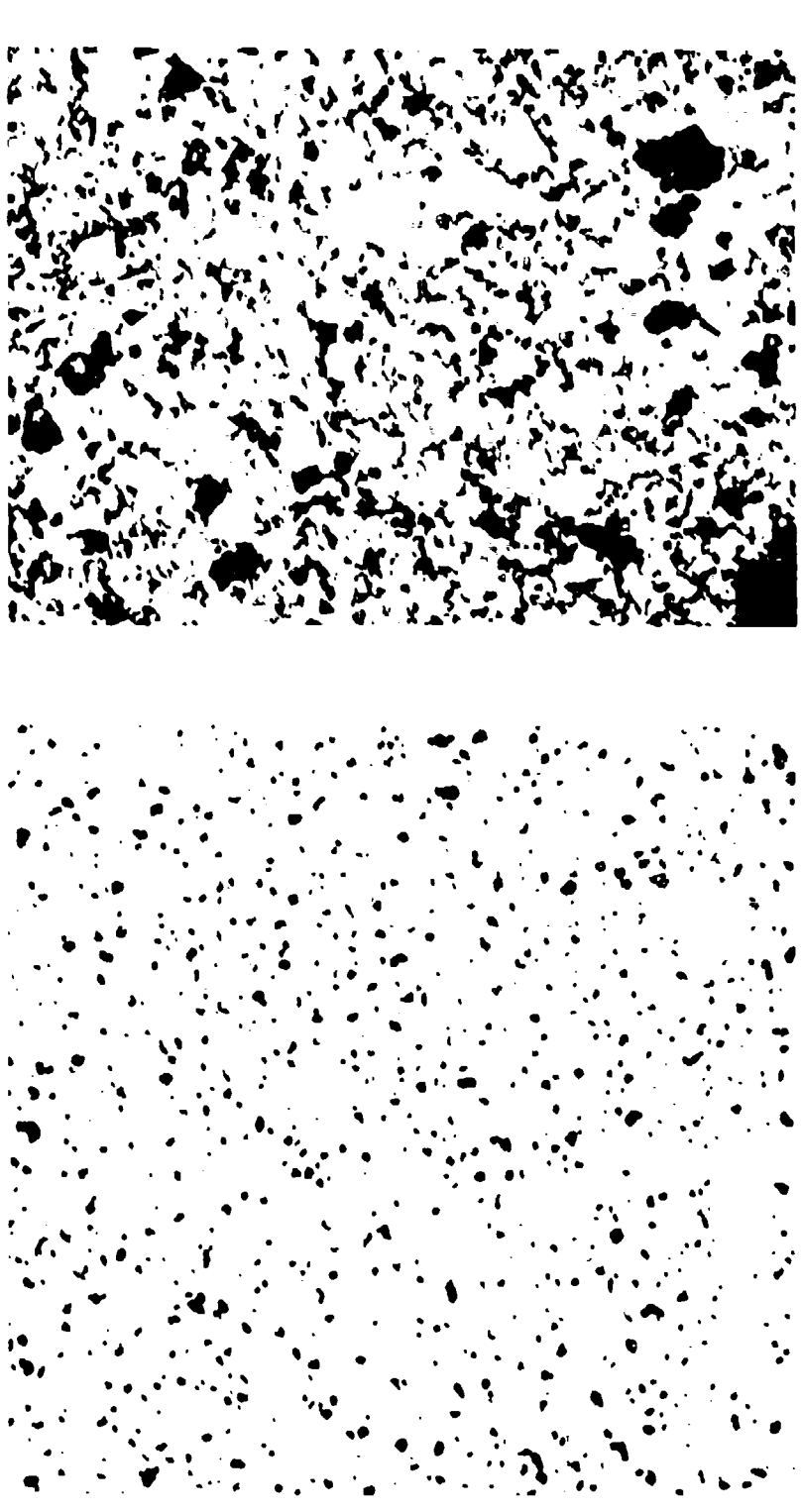

Figure 23. Sintered calcined kyanite first pressed at 69 MPa (10 000 psi) then sintered at a) 1600 ^{0}C and b) 1700 ^{0}C (75X)

Table 11

INFLUENCE OF FIRING TEMPERATURES ON CERAMIC DENSITIES

Material and Preparation	Firing Temperature (°C)	% of Theoretical Density	Number of Samples	Method[1]
F-202[2] Forsterite, pressed	1450	99.3-99.6	3	I
	1500	99.5-99.6	2	I
	1550	98.3	2	I
F-202 Forsterite, tap-dense	1450	83.2	1	I2
	1500	96.0	1	I2
	1550	97.5	1	I
C-70 Forsterite, pressed	1450	81.0-82.8	2	L
	1500	82.3-83.3	2	L
C-70 Forsterite, tap-dense	1450	78.0-81.1	1	L
	1500	85.4-86.0	1	L
"Electrical insulator"[3], pressed	1360	94.9-95.4	2	L
	1385	91.3	2	I
	1410	90.6-90.9	2	I
"Electrical insulator", tap-dense	1360	89.8-92.6	1	L
	1385	91.6	1	I
	1410	91.8	1	I
"Parian"[4], pressed	1275	89.7-92.0	2	L
	1300	91.9-92.0	2	I
	1325	91.0	2	I
"Parian", tap-dense	1275	91.1-91.7	1	L
	1300	91.9	1	I
	1325	91.1	1	I
Excel "3-5 CAL" Alumina, pressed	1875	99.2-99.4	2	I

1) L signifies use of the lacquered-sample immersion technique described in the text. I signifies the direct immersion technique, and I2 signifies use of the modified direct immersion method described in the text.
2) Nominal "maturing temperature" = 1450 °C.
3) Nominal "maturing temperature" = 1310 °C.
4) Nominal "maturing temperature" = 1225 °C.

The C-70 forsterite, expected to contain little or no glassy phase, did not sinter to a high density at the temperatures employed. Samples fired at 1600 °C melted, but were still not water-impermeable and had a lower density than those sintered at 1500 °C.

Figures 24 through 26 show the microstructures of tap-dense samples of F-202 forsterite, "electrical insulator", and "Parian" after firing to temperatures at which they absorbed no water. The microstructures are

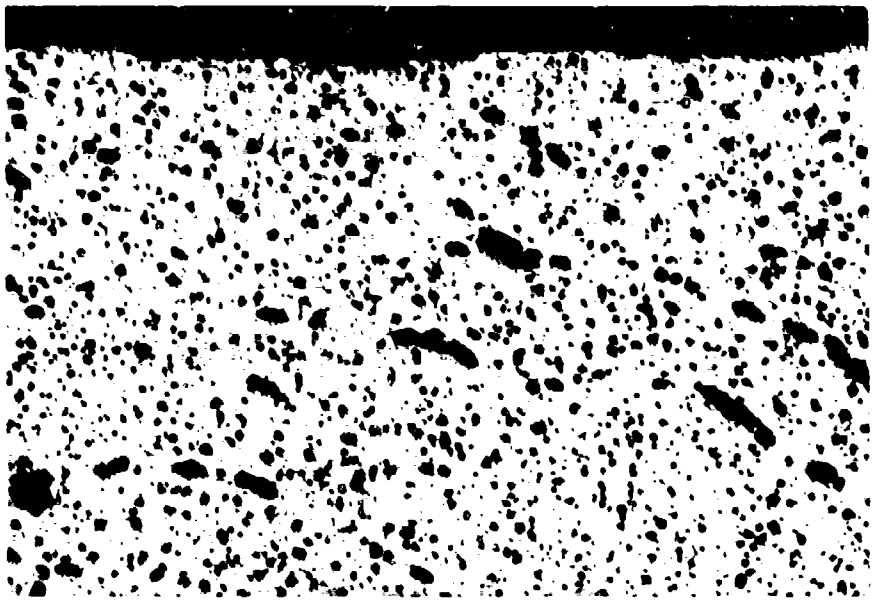

Figure 24. Tap-dense F-202 forsterite fired at 1550 °C (75X)

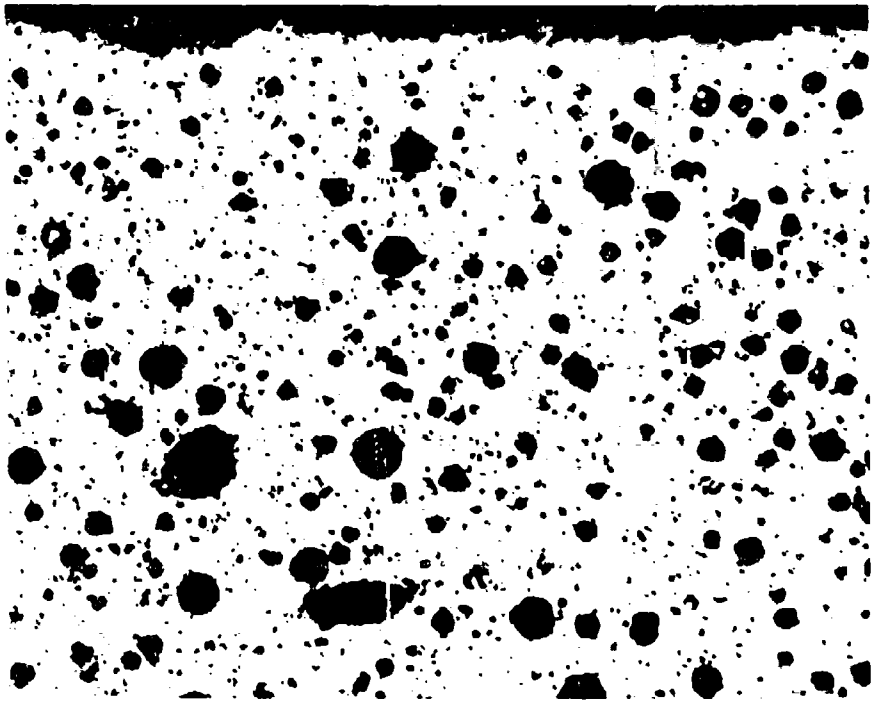

Figure 25. Tap-dense "electrical insulator" fired at 1385 °C (75X)

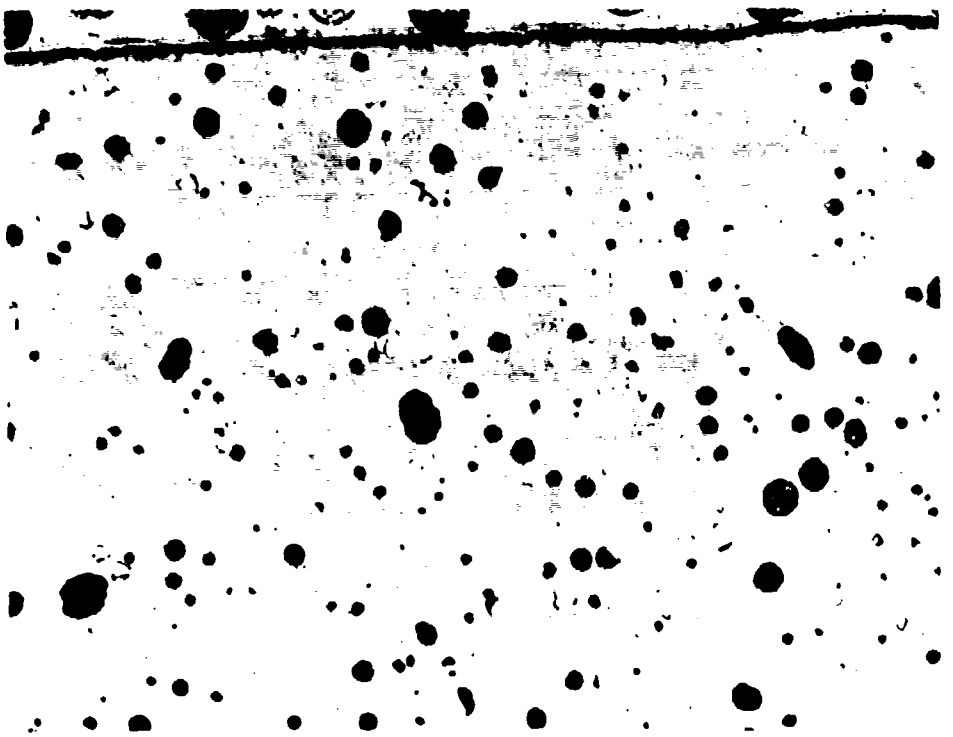

Figure 26. Tap-dense "Parian" fired at 1300 ^{O}C (75 X)

all characteristic of closed-pore materials, but the porosity differs in dimensional scale, in the order of "insulator" coarser than "Parian" coarser than forsterite.

A microtubular ceramic wall thickness of, for example, 25 to 50 μm, if magnified appropriately and represented as a pair of parallel straight lines drawn across any of the three microstructures, would have occasional through-wall pores. According to this model, the expected extent of through-wall porosity would be least for the forsterite and greatest for the coarsest microstructure, the "electrical insulator". However, examination of the upper edge of each micrograph, representing a free-edge of the sample, suggests a self-glazing of the surfaces. If the microtube wall is modeled by its magnified half-wall-thickness drawn parallel to this edge of each micrograph, there would be little or no through-wall porosity for any of the materials.

Samples of Excel "3-5 CAL" alumina, the alumina powder that was most nearly satisfactory in packed-bed powder coating (05x, 06x, and 11x series) were also fired. The firing was for 5 hours at 1875 ^{O}C in hydrogen, a treatment that would be expected to provide very high density in fine alumina powders, but not for powders as coarse as Excel "3-5 CAL". In the absence of a cylindrical metal crucible that could withstand this temperature, attempts

were made to prepare tap-dense samples 1) using a shallow pan folded up from molybdenum sheet, and 2) using a small polystyrene vial that would decompose during firing. In both instances, the tap-dense samples were unsuitable for immersion density measurements due to macroscopic cracks or interaggregate gaps. The densities of the pressed samples are shown in Table 11. The densities of these samples are surprisingly high, and their surfaces were slightly glazed, suggesting the presence of a glassy phase due to impurities. It will be recalled that several ambiguities were encountered in seeking to characterize this powder (see "Characterization of Alumina Powders", page 30). In view of the high density observed in the pressed samples of this powder, additional effort to define its significant characteristics might be warranted, as a lead toward developing more refractory microtubular structures than those permitted by the higher glass content ceramics studied in the second half of the investigation.

Section 6

MANIFOLDING EXPERIMENTS

The concept for providing manifolds for gas access to the interior of the microtubes is to seal off regions of the foam surface and then grind away part of the seal to expose the tube interiors. The surface seal might either be part of the original ceramic coating, as was illustrated schematically in Figure 1, or be provided, after firing, by a refractory cement. The integral coating would be expected to provide superior thermal capabilities, but is more difficult to develop. The principal requirement is to define a suitable ceramic paste suspension, with suitable rheology for its application to the foam surface, which will join to the partially embedded fibril powder coatings, does not crack on drying, is compatible with the remainder of the microtubular structure during firing, and does not significantly reduce its operating temperature limits. The same ceramic paste (or refractory cement) could be used to seal off surfaces in order to define flow channels in the tube-exterior region.

The concept for providing manifolds for gas access to the exterior of the microtubes is merely to leave surfaces of the foam surface open for access to the tube-exterior region, also illustrated schematically in Figure 1. The principal requirement for realizing this concept is to define a means for a) repairing surface coating damage that occurs during manipulations of the powder coating process, or b) assuring that such damage can be avoided. For example, the surfaces on which tube-external access is to be provided might be defined by holes drilled through a foam slab before the start of the powder coating process. Such surfaces would be effectively protected from accidental contact and resulting damage.

Time did not permit a thorough investigation of the manifolding requirements as part of this study, but preliminary experiments were performed in order to better define the problems involved in reducing these concepts to practice. Attempts were also made to incorporate the experimental manifolding methods in preparing sample microtubular ceramic structures for leak testing.

PRELIMINARY EXPERIMENTS ON CERAMIC PASTE SUSPENSIONS

Avoidance of cracking during the drying of a seal-coating over a microtubular ceramic surface is made difficult by the fact that the coating is partially penetrated by the rigid substrate, which obstructs shrinkage. References 9 and 10 provide excellent summaries of factors that influence the rheology, drying shrinkage, and cracking of ceramic suspensions, and means for their control. Since there was insufficient time during the current investigation for a systematic study, a number of paste suspensions were

prepared and trial coatings were made, usually on a single face of a previously powder-coated foam substrate. The pastes were made of the ceramic powders "electrical insulator", "Parian", and F-202 forsterite, from which it was desired to prepare microtubular ceramic structures for leak tests. Since the microstructures obtained during the firing studies suggested increasing likelihood of low through-wall porosity in the order of "electrical insulator", "Parian", and F-202 forsterite, it was decided to attempt the preparation of leak-test samples in that order. Accordingly, most of the initial paste suspension trials were made using "electrical insulator" powder in a variety of suspension vehicles. The following suspensions were prepared and observations concerning their performance were:

1. "Electrical insulator" powder mixture used for powder coating, plus distilled water

   This paste was very unstable, quickly separating a more fluid liquid on top when stirring was stopped. When coated on an unmodified polyurethane foam, it closed the surface but drew into the surface foam cells, creating a scalloped surface. In contrast, when coated on a previously powder-coated foam, surface tension raised the coating into a high lens-shaped configuration. It was difficult to coat, as the subsurface part of the paste quickly became overly stiff as the fluid on top separated; it was uncertain whether the foam's surface had been adequately penetrated. No cracks appeared on drying the coating on either substrate.

2. Original formulation [Ref. 9] of "electrical insulator" (containing kaolin and Kentucky ball clay) plus distilled water

   Suitable plastic rheology was observed over a range from 27.0 to 30.1 percent water, and the paste was very stable. The coating on a previously powder-coated substrate was easily controlled, with excellent penetration and smoothing characteristics. Numerous cracks appeared on drying.

3. Powder-coating mixture of "electrical insulator" plus amyl alcohol

   The suspension was "stiff" at 21.8 percent liquid and "soft" at 22.9 percent. The paste was not completely stable, but settled less rapidly than the water-base one. A previously powder-coated foam sample was coated, using paste at 22.7 percent liquid. It tended to draw into the foam slightly, making it difficult to prepare a smooth surface. Three small cracks appeared during drying.

4. Mixture of "Electrical insulator" plus amyl alcohol and benzoic acid

   The presence of weak organic acids in inorganic suspension vehicles can aid deflocculation, by positively charging the powder

particles via H^+ adsorption on their surfaces. The paste had suitable viscosity at 22.4 percent liquid, at which level the benzoic acid concentration relative to the powder was ~0.99 percent. It provided no noticeable improvement in paste stability. No coating was prepared.

5. Original formulation of "electrical insulator" plus amyl alcohol

   The suspension had suitable rheology at 27.7 percent liquid. It was more stable than the amyl alcohol paste prepared with the clay-free powder mixture of the same composition. Like the water-base suspension, many cracks developed on drying.

6. Powder-coating mixture "electrical insulator" plus isopropyl alcohol

   The paste rheology was suitable (but slightly stiff) at 22.4 percent liquid. It was more easily applied as a coating than the amyl alcohol suspension of clay-free powders (No. 3). No cracks formed on drying.

7. Powder-coating mixture of "electrical insulator" plus 25 v/o isopropyl alcohol in water

   The paste rheology was suitable (but slightly soft) at 26.7 percent liquid. The paste applied easily, and slight instability provided a fluid surface that aided smoothing of the coating. No cracks formed on drying.

   A second trial coating, made with an "electrical insulator" powder mixture plus 25 v/o isopropyl alcohol in water, also coated well and dried with no cracks.

   A coating then was made with the same paste, on a long thin slab of foam, with a 5-minute interval between coating half the slab's length and completing the coating. The objectives were: a) to test whether cracking might occur at the joint upon completing a coating of four foam faces to form a flow channel and two manifolds, as illustrated schematically in Figure 2; and b) to permit examination for cracks along the interior surface of the paste coating. The foam slab used for this experiment had been PMMA-coated, but not powder coated. It became clear that liquid absorption into the prior powder coatings had influenced the paste-coating rheology, since the paste was noticeably more fluid than in its previous applications. As a result, the coating penetrated into the foam and only thinly coated its surface. On drying, two small cracks were formed on the top surface and

one on the interior; all of them appeared to be associated with barely-coated fibrils rather than general shrinkage. Cracks of this sort should cause no leakage unless they serve as crack sources for later fracture. No crack appeared associated with the coating joint.

8. Powder-coating mixture of "electrical insulator" plus propyl alcohol

This suspension and the following one were prepared to determine whether the favorable results obtained with isopropyl alcohol might be duplicated with a less volatile related suspension vehicle. The paste rheology was slightly stiff at 21.8 percent liquid, and about right at 22.2 percent. On drying, one small crack formed with a coating made of this suspension.

9. Powder-coating mixture of "electrical insulator" plus 25 v/o propyl alcohol in water

The paste rheology was slightly stiff at 24.9 percent liquid, and a little soft at 25.5 percent. A coating made with 25.3 percent liquid was difficult to smooth, tending to a dry surface. No cracks formed when it dried.

10. F-202 forsterite plus 25 v/o isopropyl alcohol in water

The paste rheology was suitable for use at 27.6 percent liquid. It was much more stable than the pastes prepared with the "electrical insulator" powder coating mixture and resembled the clay-containing paste. It coated well, but without the fluid-surface characteristic. No cracks formed on drying.

11. Powder-coating mixture of "Parian" plus 25 v/o isopropyl alcohol in water

The paste rheology was suitable (but a little stiff) at 24.9 percent liquid. The coating behavior was similar to that with the "electrical insulator" mixture, including the fluid-surface characteristic. No cracks formed during drying.

12. Powder-coating mixture of "electrical insulator" plus 25 v/o isopropyl alcohol and 1.6 percent polyvinyl alcohol* in water

PVA was included in the vehicle for this suspension in order to provide approximately 0.5 percent as a binder in the final coating.

*Dupont Elvanol 51-05 PVA

since the previously prepared coatings were quite powdery. The paste rheology seemed suitable for use at 27.0 percent liquid, but it was a bit stiff in actual coating. Its stability seemed similar to the analogous paste No. 7 without PVA, but it lacked the "fluid surface" characteristic during application. No cracks formed on drying. The dried coating could be rubbed with the fingers with no visible rub-off of powder.

In order to explore suitable (nonsticking) supports for drying fully coated foam samples, a bit of paste No. 12 was placed on surfaces of paraffin, Teflon, and polyvinyl chloride. After about one hour, the partly dried paste could be moved with little loss on either the Teflon or polyvinyl chloride surfaces, but adhered to the paraffin.

Drying time measurements were made on many of the trial coatings, and are shown in Figure 27. Surprisingly, the rate of liquid loss from the isopropyl alcohol-water pastes is no higher than from the propyl alcohol-water pastes, despite the difference in their water-free counterparts.

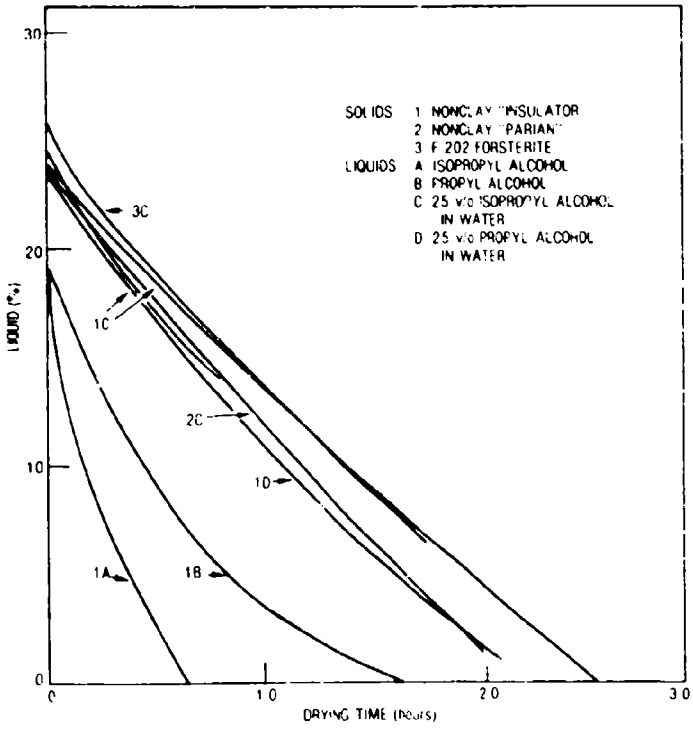

Figure 27. Room-temperature evaporation of liquid from single-side coatings of paste suspensions on powder-coated foam samples

The preliminary experiments on ceramic paste suspensions suggested that satisfactory crack-free coatings might be prepared with suspensions of the "electrical insulator" or "Parian" powder-coating mixtures or F-202 forsterite powder, in a vehicle of 25 v/o polyvinyl alcohol in water. It also appeared that approximately 0.5 percent PVA in the coating, introduced via the vehicle, would provide a coating with enhanced strength for convenient handling, with only minor influence on coating behavior of the paste. It appeared that the joint formed after a modest amount of drying of a coating, when four surfaces of a sample are coated, would not lead to cracking, and that the coated sample could be supported on a Teflon or PVC surface to dry. Further experiments will be discussed in a following section on the preparation of manifolded samples for leak testing.

TUBE-EXTERIOR MANIFOLDS: PRELIMINARY EXPERIMENTS

Experiments were conducted seeking to establish a method, analogous to the packed-bed powder coating process, to coat ceramic powder onto uncoated substrate fibril tips at sample surfaces to provide gas access to the microtube exterior region.

In order to provide a means for supplying adhesive to the surface fibril tips, a dry inkpad of fine-pore foam was saturated with a solution of 4 ml heptane/g S-10 terpene resin, the same solution used for adhesive coating in the packed-bed process.

A face of a previously powder-coated foam sample was moistened by contacting the saturated pad, then placed in contact with the surface of a bed of F-202 forsterite powder. On removal, it was found that the sample's surface was largely bridged over with powder, rather than it adhering only to the fibril tips. The procedure was repeated, but allowing approximately two minutes for evaporation of solvent from the adhesive coating before contacting the forsterite powder bed. Again, the surface was largely bridged over.

The foam sample was then placed in the screen-faced tongs of the Dremel vibrator used for removal of nonadherent powder in the packed-bed coating process. The screens contacted sample faces previously coated with paste suspensions. On turning on the vibrator, excess powder was removed from the lateral face satisfactorily, but the vibrating screen faces also removed a substantial portion of the paste coatings in contact with them.

The procedure was repeated, but using as the foam sample the one previously paste-coated with the PVA-strengthened suspension (No. 12). There was no discernible loss of powder from this paste-coated surface.

PREPARATION OF SAMPLES FOR LEAK TESTING

"ELECTRICAL INSULATOR"

Based on the preliminary manifolding experiments, the foam sample previously powder-coated with the "electrical insulator" powder mixture (29x series) was coated on four faces with a paste suspension of the same powder in 25 v/o isopropyl alcohol plus 1.6 percent PVA in water. The liquid content was 26.9 percent, producing an average PVA concentration of 0.58 percent in the dried coating. The paste seemed somewhat stiff in application. Nevertheless, when the paste-coated sample was placed on a Teflon sheet to dry, paste flowed out slightly at the edges under the influence of the sample's weight.

The drying rate of this sample was approximately half that observed in the single-face coating experiments (Figure 27), suggesting that drying from the inner surfaces of the paste coatings is impeded when four faces are sharing that region for evaporation. After 3/4 hour of drying, a crack was observed, extending from one edge to the center of the top face. At that time, the calculated average liquid content of the coating was 20.4 percent, but the top face was presumably drier than that level. On completion of drying, the crack on the top face had opened wider but not noticeably extended. Two additional cracks had formed along the lower edges, in the flowed-out paste in contact with the Teflon support. On chipping off these flowed-out edges, it was found that these cracks ran roughly parallel to the lower surface, entirely within the paste coating, and did not intersect the underlying powder-coated foam.

The lower face, dried in contact with the Teflon support, was slightly powdery, while the three faces from which free evaporation (and thereby PVA enrichment) occurred were not.

In order to repair damaged coatings on the fibril tips of the two faces left open (not paste-coated), they were contacted to the S-10/heptane saturated foam pad, dried approximately two minutes, contacted to a bed of "electrical insulator" powder, and then vibrated in the screen-faced tongs. The sample's lateral faces, both dried in the open, were placed in contact with the screen faces to avoid grinding away the powdery lower face of the sample. The sample was then placed in the oven at 130 °C for 15 minutes. Visual observation indicated that one face was quite poorly repaired, the other fair, with a few bare fibril tips.

The entire process was repeated, but with 15-minute drying of the S-10/heptane solution, a 30-minute hold time between contacting the powder and the vibratory shake-out, and a 30-minute consolidation in the oven.

Thus, the times were made equal to those used in packed-bed powder coating, except for the S-10 application*. Visual observation indicated little improvement.

The process was repeated, but without additional S-10 application, as in the repeat cycles of the packed-bed powder coating process. The sample was pressed more firmly onto the powder bed, deliberately building up an adherent cake of compressed powder. After shake-out and oven consolidation, visual observation indicated considerable improvement, but the fibril tip coatings were not quite continuous.

The process was repeated once more. Visual observation indicated a few dark areas, but they were considered no worse than at least one visible internal defect, a small crack in a fibril coating.

Results of firing the sample will be presented in a subsequent section.

"PARIAN"

In view of the cracking observed on drying the "electrical insulator" paste coating, contrary to results of the preliminary test coatings, some additional experiments were performed before paste-coating the "Parian" powder-coated sample. A review of the previous single-face coating experiments indicated that their typical dried coating weight per face was similar to that of the four-face coated sample. Most of the samples had only one quarter to one half as much powder-coating thickness, and hence might have withdrawn less liquid from the paste; however, the single-side coating made with the same paste (preliminary coating No. 12) had approximately the same powder-coating thickness as the four-face coated sample. As mentioned before, the four-face coated sample dried more slowly, and the top and lateral faces probably dried predominantly from the outside rather than via both external and internal surfaces. As a result of this review, it was tentatively concluded that "strengthening" of the paste by the addition of PVA, perhaps aggravated by unidirectional drying, was most likely responsible for the cracking. It was reasoned that a powdery coating separates particle-to-particle as it dries (like sand), whereas a "bonded" coating cracks (like mud) to accommodate shrinkage strains. Accordingly, experiments were undertaken to see if a coating might be strengthened after drying, to render it capable of withstanding the vibration used in repairing the "open" faces.

The application of either a polystyrene/toluene lacquer solution or a water-base glue to previously prepared PVA-free single-face paste coatings

*In the packed-bed powder coating process, 30 minutes was allowed for drying the S-10/heptane solution, primarily to assure an accurate weight, used as the basis for assessing subsequent powder additions.

caused the coatings to curl and peel away from the underlying portion of the coating as the lacquer or glue dried. A low-viscosity epoxy was then applied to two opposite faces, previously single-face paste coated. No curling or delamination was observed on curing the epoxy (20 min at 60 °C), and it was planned to use this material and procedure for coating the "Parian" sample.

The foam sample previously coated with the "Parian" powder mixture (30x series) was coated with a paste suspension of that powder plus 25 v/o isopropyl alcohol in water. The liquid content was 26.3 percent. Great difficulties were encountered in applying this coating. While initially the coating seemed quite stiff, by the time the fourth face was being coated it had developed a strong tendency to creep-flow while still appearing relatively stiff at the higher shear rates used in the coating operation itself. This characteristic, known as dilatency, is a rheological behavior often observed in coarse-particle or flocculated suspensions [Ref. 9].* Presumably in the early part of the coating operation, liquid absorption into the powder coating on the fibrils kept the paste stiff enough to prevent creep flow. By the time the fourth face was reached, the powder coating was probably about saturated, and no longer withdrew liquid from the paste. The coating process was interrupted for 15 minutes, since the creep flow became so severe that the coating configuration could not be controlled. The final coating was excessively thick, in some places penetrating quite far into the foam interior. Visual inspection confirmed the liquid absorption by the fibrils'powder coating, since it had acquired a smooth surface.

The sample was placed on a flexible polyurethane open-cell foam support to dry, and dried without cracks. The drying rate was even slower than for the "electrical insulator" four-side coating, no doubt because of the greater coating thickness.

After drying, the sample was coated with the low viscosity epoxy previously tested. After curing, the surface was still slightly powdery so a second coat was applied and cured.

The sample's open faces were moistened with S-10/heptane solution and dried 15 minutes. On pressing these faces into the bed of "Parian" powder to repair any damaged tip coatings, cracking was observed between the epoxy-permeated part of the paste coating and the unpenetrated powdery portion adjacent to the underlying foam. The external coating was removed, but leaving the considerable portion that had penetrated into the foam sample intact.

*Flow-out of the "electrical insulator" coating at the bottom face in contact with the Teflon support is probably an indication of dilatency, though less severe, in that suspension.

The repair of damaged tip coatings was continued, using the procedure finally adopted for the "electrical insulator" sample. It was planned to epoxy over the previously paste-coated faces after firing, in order to simulate that coating for preparation of a tube-interior manifold for leak testing.

Results of firing the sample will be presented in a subsequent section.

F-202 FORSTERITE

In view of the difficulties encountered in coating four sides with PVA-free "Parlan" paste, a trial single-face coating was made with F-202 forsterite powder suspended in a 25 v/o isopropyl alcohol/water solution with about 0.3 percent PVA, one fifth that used for the "electrical insulator" suspension. The suspension spread very easily, but two cracks developed during drying.

Another trial single-face coating of F-202 forsterite powder plus 25 v/o isopropyl alcohol in water (no PVA) also cracked on drying. A single-face coating of F-202 plus 28.4 percent water developed some very short cracks at the edge, but they did not grow.

It was decided to try a procedure of first repairing damaged fibril-tip coatings on the faces to be open for tube-exterior gas access, then paste-coat the other faces without touching the open faces. With this order of processing steps it is not necessary to provide a paste coating that can withstand vibration in the tip-repair procedure. However, it does require partial drying between paste-coating adjacent faces, with a possible risk of cracking at the joints between the faces.

The open faces were powder-coated, four cycles, using the procedure described for the "electrical insulator" sample. Tip coatings appeared continuous.

The paste suspension prepared initially with 28.4 percent w[illegible] appeared somewhat stiffer after 24 hours, and was diluted to 30.0 percent [illegible] coating procedure was:

1) Holding the sample between opposite faces, designated 3 and 4, coat face 1.

2) Dry 5 minutes to assure against sag on inverting.

3) Invert and coat the opposite face, 2.

4) Dry 20 minutes, so faces 1 and 2 can be handled.

5) Holding the sample between fac[illegible] 1 and 2, coat face 3.

6) Dry five minutes to assure against sagging.

7) Invert and coat face 4.

The coating procedure was reasonably satisfactory, although the suspension was rendered a little soft by diluting to 30 percent water. The result was some surface-tension related difficulties in assuring penetration into the foam structure, and a slight tendency to creep-flow, for one or two minutes after coating faces 3 and 4. The joints between the faces caused no problems, either in the coating process or on drying. However, numerous cracks appeared on the top face (4), and several smaller cracks formed on the bottom face (3) on drying. Figure 28 shows the cracks on face 4. No cracks appeared on either of the lateral faces, but at the corresponding time interval (28 minutes after coating) when cracks were first observed on face 4, the sample was being held between faces 1 and 2 for coating. It is possible that faces 1 and 2 contained subsurface cracks, smeared over at the surface, but, if so, they did not spread to the surface on further drying.

Figure 28.

Drying cracks on top face of F-202 forsterite paste suspension coating (6.5X)

The F-202 forsterite paste suspension behaved much like a clay-containing suspension. It was stable against separation of liquid, displayed a very "plastic" rheology, with little or no dilatency; and formed numerous cracks on drying. This behavior is surprising, since the powder was prepared from material prefired one hour in air at 1180 ^{o}C. At this temperature, kaolinite has long since dehydrated, and has decomposed to a 1:1

mullite-type phase plus SiO_2 as cristobalite [Ref. 11]. The clay-like behavior may derive from retention of the original distribution of particle sizes despite the extensive changes in structure.

While the paste suspension used was unsatisfactory because of its drying cracks, the coating procedure used on this sample was more satisfactory than that used for the first two samples, and provides a possible basis for developing an acceptable manifolding process.

Ref. 11 G.W. Brindley and M. Nakahira, "A New Concept of the Transformation Sequence of Kaolinite to Mullite," Nature, Vol. 181, 1958, pp. 1333-1334.

Section 7

FIRING OF LEAK TEST SAMPLES

"Electrical insulator" tap-dense samples previously fired at both 1385 and 1410 °C had shown no significant water absorption, and pressed samples fired at both temperatures displayed a light glazing of the surface but no loss of sharpness at their edges. Accordingly, it was decided to fire the coated foam sample for one hour at 1410 °C. The sample was fired on a setter of bubble zirconia, screened to -35 + 60 mesh, which had previously been tested as a nonsticking support for an F-202 forsterite sample fired at 1550 °C.

On removal from the furnace, the sample was found to be severely overfired. Its surface was heavily glazed, and part of the bubble zirconia setter was firmly attached by the excess glass. The external configuration had sagged, with approximate shrinkages of 27 percent vertically and 14 to 17 percent* horizontally. Part of the microtubular structure visible on the "open" faces appeared to have been removed by surface tension effects, as shown in Figure 29.

No explanation has been found for the apparent discrepancy between the test firing and the results of this firing, performed in the same furnace approximately three weeks later. However, no test firings were performed on this ceramic at temperatures above 1410 °C. Consequently, there was no knowledge of the margin available for temperature errors.

"Parian" tap-dense samples previously fired at both 1300 and 1325 °C displayed no significant water absorption. The samples fired at 1325 °C were more heavily glazed than those fired at 1300 °C, but no rounding of the edges was observed after firing at either temperature. In view of the overfiring experience with the "electrical insulator" sample, the "Parian"-coated foam sample was fired for one hour at 1300 °C. On removal from the furnace it was found that the sample had sagged, far more than the "electrical insulator"-coated sample. Like that sample, it was heavily glazed, and bubble zirconia setter was firmly attached to its base. It was not considered worth attempting to leak-test this severely slumped sample.

The F-202 forsterite tap-dense sample fired at 1550 °C displayed no significant water absorption, while that fired at 1500 °C showed a 0.2 percent weight gain after soaking five minutes in water. Firings at these temperatures were monitored by optical pyrometry, rather than by thermocouple.

*The ratio of the fired and green densities for tap-dense "electrical insulator" corresponds to a linear shrinkage of 16 percent.

Figure 29.

"Open" faces of "electrical insulator" microtubular structure after firing at 1419 °C. (6.5X)

In view of the experience with the earlier samples, the firing instruction for the F-202 forsterite-coated foam sample was to observe the sample edge with the pyrometer, and commence cooling at the first sign of sagging, or on reaching 1525 ^{o}C, whichever occurred first. When the sample was first hot enough for observation, about 800 ^{o}C, it was seen to have collapsed. It was clear that, at least in this sample, the ceramic's green strength, in the temperature ranges where the polymer substrate decomposes (250 to 500 ^{o}C), was insufficient for the microtubular portion of the structure to support the weight of the solid external coating. Insufficient low-temperature strength may also have contributed to the sagging found in the earlier firings.

Alternatives are available to remedy the difficulties associated with insufficient low-temperature strength, but time did not permit testing these procedures in the present investigation. The most direct method would be to fire samples without a surface coating, and use a refractory cement, applied after firing, to form flow channels and tube-interior manifolds. Use of refractory cement would cause some sacrifice of maximum operating temperature. Another possible procedure would be to prefire samples without a surface coating to a temperature sufficient to provide enhanced strength but little shrinkage. The required external coatings could then be applied and high-fired along with the microtubular portion.

Section 8

LEAK TESTING

The adhering bubble zirconia setter was ground off the lower face of the "electrical insulator" microtubular ceramic. Its apparent density was then determined by immersion, in order to provide at least a rough estimate of the extent of enclosed microtubular volume. (In view of the sample's overfiring, it was considered possible that the tubes might be entirely closed.) During the immersion weighing, the sample weight increased, over a two-minute interval, by an amount corresponding to a reduction of ~ 0.01 percent of the displaced volume. This observation demonstrated qualitatively that there was at least some internal void space and some leakage into it. The measured apparent density was 2.312 g/cm^3, corresponding to a void volume of 0.028 cm^3 (0.0017 in.^{3}) if the solid portion's density was that observed for the 1410 ^{o}C tap-dense test firing. Assuming a 16 percent linear shrinkage from the unsintered fibril diameters, the estimated microtube internal cross-sectional area is about 5 x 10^{-4} cm^2 (7.7 x 10^{-5} in.^{2}). Hence, the estimated length of the microtubes in the sample is about 56 cm* (22 inches), or 12 percent of the estimated 486 cm (16 feet) the sample should contain if undamaged.

In order to establish a selective access to the tube interiors, a 0.635-cm (0.25-inch)-diameter hole was ultrasonically bored into the sample's lower face. With the marginal illumination and hand-lens observation used, there was some uncertainty in distinguishing microtube openings from possible bubbles in the paste suspension coating. Microtube openings may have been encountered at a depth of 0.102 cm (0.040 inch). By keeping track of hole locations, it was assured that the microtubes had been intersected at a depth of 0.127 cm (0.050 inch). At this level, there was an apparent "shadow" of another microtube opening visible through the translucent ceramic, and boring was continued to a depth of 0.132 cm (0.052 inch). At this depth, the base of the boring had broken through the bottom of the coating in a small hole. Figure 30 shows the bored-out face of the sample.

Positive means to avoid such breaking through the paste-suspension coating is one of the features needed in an acceptable process for providing tube-interior manifolds. A suitable means might be to first apply a coating that is "troweled in" flush with the substrate surface, then apply additional coating only to those areas to be used for seals. This approach would assure

*The estimate of microtube length is, unfortunately, very sensitive to the assumed density of the solid, since the solid-to-void ratio is very large. If it were assumed that, due to overfiring, the solid density is the ceramic's estimated theoretical density, the calculated microtube length would be ~350 cm (11 feet), or 72 percent of the estimated length if undamaged.

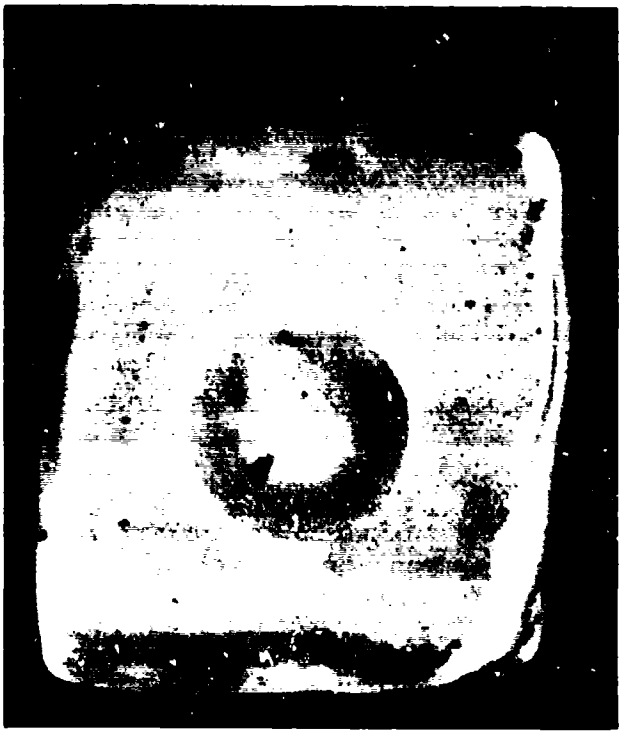

Figure 30.

Bored-out face of electrical insulator" microtubular sample. Openings into microtube interiors are visible at the base of the hole, as well as the break through the coating, located at about 7 o'clock. (6.5X)

that a very light grinding would suffice to open up the tube interiors in the regions planned for use as manifolds.

The break through the coating base was repaired with epoxy, and the sample was sealed with Apiezon sealant onto the test opening in a vacuum system, equipped with a calibrated leak, used for leak testing of vacuum apparatus. The resulting vacuum level was greater than 500 μm Hg (67 Pa), indicating too great a leak rate for measurement with this apparatus.

A manometer and flowmeter apparatus was then constructed to measure the flow rate through the sample's leaks under a small pressure differential from atmospheric pressure. The flow rates observed varied approximately linearly with pressure differential, at a ratio of 0.0051 $cm^3 \cdot s^{-1} \cdot Pa^{-1}$ (0.16 SCFH/inch of water). Applying the equation for laminar flow through tubes, using the estimated total microtubular cross-sectional area for the sample's size, and taking the flow length as 1.5 x the nominal length, the calculated ratio of flow through the tubes per unit pressure differential is 0.068 $cm^3/\cdot s^{-1} \cdot Pa^{-1}$ (2.1 SCFH/inch of water), for room temperature air at one atmosphere. Hence, the leak rate of this sample is approximately 7.5 percent of its design flow rate for the same pressure differential. For context, this ratio is similar to that typical of rotating ceramic honeycomb regenerators in the sizes used with experimental automotive gas turbines. The leakage of this single sample cannot, of course, be regarded as "typical" of the potential for microtubular ceramic heat exchangers.

After completion of the leak tests, the sample was mounted in epoxy and sliced in two to permit examination of its interior. The region below the sagged upper face (as oriented during firing) was almost entirely devoid of microtubes. The lower region adjacent to the tube-interior manifold was reasonably occupied by microtubes. These observations confirm qualitatively the microtube content estimated from the sample density.

Section 9

SUMMARY AND CONCLUSIONS

SUMMARY

Calculations and experiments were conducted to explore the feasibility of producing very compact high-temperature heat exchangers via microtubular ceramic structures. Such microtubular ceramic structures consist of multiple interconnected ceramic tubes with very thin walls, small diameters, and modest ratios of length to diameter. As a result, they should have reasonable strength, as well as very high specific area. The investigation included: calculations of expected volume requirements and heat-exchange performance for microtubular ceramic heat exchangers compared to ones of conventional dimensions; experiments seeking to define means for preparing leak-tight microtubular ceramic structures; preliminary exploration of means to provide separate manifolds to the interior and exterior of the microtubes; and a leak test of one experimental microtubular ceramic structure including such manifolds.

Heat-transfer calculations were performed for six assumed ceramic materials, in order to assess their suitability for use in microtubular heat exchangers and to test the validity of earlier specific volume estimates made via a partial heat-exchange analysis. It was found that, for the six materials examined:

- The choice of material should make little difference to thermal performance
- Both the heating and cooling effectiveness factors for microtubular heat exchangers should exceed those for conventional ones
- The specific volumes of microtubular heat exchangers should be smaller than conventional exchangers by a factor of ~ 21 to 29, depending on the assumed materials and heat-exchange fluids and the calculation methods employed.

It was also found that steady-state thermal stresses should be much smaller for microtubular ceramic heat exchangers than for conventional exchangers, and should not limit the maximum allowable initial temperature difference of the heat-exchange fluids. The calculated maximum permissible fluids temperature difference was slightly higher for microtubular ceramic heat exchangers than for conventional exchangers made of the same material. No major alterations in these relative comparisons resulted from alterations of the assumed operating parameters or changes in the calculation method.

The experimental approach for preparing microtubular ceramic structures was based on coating ceramic powders on a sacrificial substrate,

consisting of polyurethane foam modified by the addition of polymethyl methacrylate to convert the foam fibrils to round cross sections. The ceramic coatings were prepared by: 1) embedding an adhesive-coating substrate in a packed bed of dry powder which infiltrates into the foam, 2) allowing time for the adhesive to accrete powder to the substrate, 3) shaking out nonadherent powder from the foam interstices, 4) consolidating the coating by heating, and 5) repeating this sequence until adequate thickness was achieved. Coatings were monitored by microscopic observation, as well as weight gain, to assess their uniformity and continuity.

Some refinements of the packed-bed powder coating process were introduced during the investigation. The primary focus, however, was on exploring the suitability of various ceramic powders for use in the process, with the process parameters held fixed to permit comparison among the powders. The initial experiments were conducted mainly with a variety of alumina powders. From these experiments, it was concluded that the most important characteristic of powder behavior in this coating process is its tendency to form aggregates. The tendency to form aggregates increases with finer particle-size powders, needed for sintering pure oxide ceramics to a high density. None of the alumina powders tested was completely free of aggregate formation problems, and the most nearly satisfactory one contained rather coarse particles.

In view of the results on alumina powders, experimental coating efforts were shifted to powders that might be used to formulate ceramics in the Al_2O_3-MgO-SiO_2 system, plus fluxes. The objective was to enhance the likelihood of achieving satisfactory sintering, while using coarse particle-size powders that would not form aggregates during the powder coating process. Fourteen "candidate constitutent" powders and two preformulated ceramic powders were investigated. Among them, powders were found with both satisfactory powder coating behavior and sufficient divergence of composition to permit reformulating a variety of conventional ceramics in the Al_2O_3-MgO-SiO_2 system. Two powder mixtures prepared from constituents that behaved well in the powder coating process also produced satisfactory coatings.

Firing studies and density measurements were made on the two preformulated ceramic compositions and the two powder mixtures, as well as partial studies on one of the "constituent" powders alone and on the most nearly satisfactory-coating alumina. Tap-dense samples were fired, as well as pressed ones, in order to simulate the sintering behavior of the low green density structures expected in powder-coated foam samples. Suitable firing temperatures, judged by high density and no significant water absorption of the initially tap-dense samples, were defined for one of the preformulated ceramic compositions and for both of the powder mixtures. Micrographic examination of a section through the free surface of the fired tap-dense samples showed a self-glazing action, suggesting that the microtubular

ceramics might be leak-tight despite the existence, farther from the surface, of pores comparable in size to the desired microtube wall thicknesses.

Ceramic paste suspensions were explored, for use in coatings to define flow channels and provide for manifolds for access of gases to the interior of the microtubes. There was insufficient time to develop suspensions that had satisfactory rheology for coating and also would reproducibly dry without crack formation.

A procedure was defined for repairing surface damage to fibril tip coatings for use on "open" faces which serve as manifolds for gas access to the microtube exteriors. The process is analagous to the packed-bed powder coating process, but utilizes a pressed-on cake of powder on the surfaces being repaired in place of the packed bed of powder penetrating the foam's interstices.

Three powder-coated foam samples were prepared with paste suspension coatings on four faces and the other two faces prepared so as to serve as tube-exterior manifolds. On firing, one of the samples was overfired and sagged considerably, a second was overfired and sagged, beyond use, and the third collapsed while still at a relatively low temperature. These results indicate that at least the third material had insufficient green strength, in the temperature range of substrate decomposition, for the microtubular portion to support the heavy paste suspension coating. Insufficient green strength may also have contributed to the sagging of the overfired samples. Alternative procedures have been suggested to circumvent this problem, but have not been tested.

Immersion measurement of the apparent density of the "considerably" sagged overfired sample provided a very rough estimate of the extent of the open microtubes remaining, ~12 percent of the estimated 480 cm (16 feet) of microtube length it should contain. Measurement of the leakage rate through pores or (more likely) gross defects in this microtubular structure indicate a leakage equal to ~ 7.5 percent of the expected flow rate through the microtubes for the same pressure differential.

CONCLUSIONS

Satisfactory powder coating can be accomplished for preparation of microtubular ceramic structures in the Al_2O_3-MgO-SiO_2 system. It is believed that low-leakage structures could be prepared by firing microtubular ceramic structures of these compositions. A good basis has been established for the development of processes required to provide manifolds for selective access to the microtube exteriors and interiors. Problems have been defined, and possible approaches to their solution have been identified but not yet tested. The leakage rate between the microtube's exterior and interior, for the single sample tested, was comparable to that of state-of-the-art rotating honeycomb regenerators.

Section 10

REFERENCES

1. H.B. Vakil, An Analysis of the Foam Heat Exchanger, unpublished work.

2. S.P. Timoshenko and J.N. Goodier, Theory of Elasticity, 3d edition, McGraw-Hill Book Company, New York, 1970.

3. J.G. Knudsen and D.L. Katz, Fluid Dynamics and Heat Transfer, McGraw-Hill Book Company, New York, 1958.

4. W.H. McAdams, Heat Transmission, 3rd edition, McGraw-Hill Book Company, New York, 1954.

5. R.A. Bowman, A.C. Mueller, and W.M. Nagle, "Mean Temperature Difference in Design", Transactions of the ASME, Vol. 62, 1940, p. 283.

6. A.S.T. Thomas et al., "Variation in Heat-transfer Rates Around Tubes in Cross Flow", Proceedings of the General Discussion on Heat Transfer, the Institution of Mechanical Engineers, 1951, p. 177.

7. R. Papin, "Bentonite", Encyclopedia of Chemical Technology, 2nd edition, John Wiley & Sons, Inc., New York, Vol. 3, 1964, pp. 339-360.

8. L. Navias, "Advances in Ceramics Related to Electronic Tube Developments", Journal of the American Ceramic Society, Vol. 37, 1954, pp. 329-350.

9. F.H. Norton, Elements of Ceramics, Addison-Wesley Publishing Company, Reading, Mass., 1952.

10. W.D. Kingery, Introduction to Ceramics, John Wiley & Sons, New York, 1960.

11. G.W. Brindley and M. Nakahira, "A New Concept of the Transformation Sequence of Kaolinite to Mullite", Nature, Vol. 181, 1958, pp. 1333-1334.

Section 11

DISTRIBUTION LIST

Addressee	DODAAD Code	Number of Copies
Scientific Officer Administrative Contracting Officer Director, Naval Research Laboratory Attn: Code 2627 Washington, D.C. 20375	N00014 S0701A N00173	3 1 6
Defense Documentation Center Building 5, Cameron Station Alexandria, Virginia 22314	S47031	12
Commanding Officer Office of Naval Research Branch Office Building 114, Section D 666 Summer Street Boston, Massachusetts 02210	N62879	1
James C. Goodwyn Defense Advanced Research Projects Agency 1400 Wilson Boulevard Arlington, Virginia 22209		1
Dr. Robert Ruh Metals and Ceramics Division Air Force Materials Laboratory Wright-Patterson Air Force Base, Ohio 45433		1
Dr. Glen Benson Energy Research and Generation, Inc. Lowell and 57th Street Oakland, California 94608		1

END 9-79